

# Towards low-cost, environmentally friendly printed chalcopyrite and kesterite solar cells

Cite this: *Energy Environ. Sci.*, 2014, 7, 1829

Hamed Azimi,<sup>\*a</sup> Yi Hou<sup>ac</sup> and Christoph J. Brabec<sup>ab</sup>

Received 27th November 2013  
Accepted 5th March 2014

DOI: 10.1039/c3ee43865a

www.rsc.org/ees

Solution-processed organic and inorganic semiconductors offer a promising path towards low-cost mass production of solar cells. Among the various material systems, solution processing of multicomponent inorganic semiconductors offers considerable promise due to their excellent electronic properties and superior photo- and thermal stability. This review surveys the recent developments of "all solution-processed" copper–indium (–gallium)-chalcogenide ( $\text{CuInS}_2$ ,  $\text{CuInSe}_2$  and  $\text{Cu}(\text{In}, \text{Ga})(\text{Se}, \text{S})_2$ ) chalcopyrites and copper–zinc–tin-chalcogenide ( $\text{Cu}_2\text{ZnSnS}_4$  and  $\text{Cu}_2\text{ZnSnSe}_4$  (CZTS(e))) kesterite solar cells. A brief overview further addresses some of the most critical material aspects and associated loss mechanisms in chalcopyrite and kesterite devices. Today's state-of-the-art performance as well as future challenges to achieve low-cost and environmentally friendly production is discussed.

## Broader context

Photovoltaics as the only truly portable renewable-energy conversion technology available today demonstrate strong commercial growth and hold promise for significant market opportunities. Among various solar cell technologies, thin-film technologies are one of the cost-competitive solar technologies due to reduced material and fabrication costs. However, the production of thin film solar cells typically relies on capex intense vacuum-based techniques, and/or high-temperature processes, both increasing manufacturing costs. Solution processing of multicomponent inorganic solar cells is considered as a promising alternative fabrication route to the conventional high cost vacuum techniques.

## 1. Introduction

Thin film solar cell technology has a major potential for further cost reductions, provided that the expected increases in production facility size and efficiency are realized.<sup>1–3</sup> Fig. 1 compares the world record single cell efficiencies of various types of thin film solar cell technologies including organic, inorganic and hybrid semiconducting materials. Among the various types of thin-film solar cells,  $\text{Cu}(\text{In}, \text{Ga})(\text{Se}, \text{S})_2$  (CIGSse) is today the combination that delivers one of the highest power conversion efficiencies. The CIGSse world record efficiency above 20% was only recently demonstrated,<sup>4,5</sup> and highlighted how close CIGSse already is to poly-Si technology. Although CIGSse technology has a number of attractive features, the deposition of the absorber layer is a complex process requiring vacuum technologies. The common approach for the production of copper indium gallium diselenide (CIGSe) solar cells is currently based on the co-

evaporation of individual metallic elements or on sputtering of the suitable metal precursors followed by a crystallization step at high temperature in the presence of Se vapor and/or hydrogen selenide gas (known as depositon-reaction or a sequential process). These processes are generally challenging due to the difficulty to control the film composition over a large area and the use of toxic gases for selenization. Over the past few years, the quest for low cost production focused more and more towards the non-vacuum deposition methods. The non-vacuum approaches for deposition of multicomponent inorganic absorber layers can be generally summarized under three main categories: (i) solution deposition based on electrochemical and chemical bath-based techniques like electrodeposition, electroplating and chemical bath deposition (CBD). (ii) Printing/coating from molecular-based precursor solutions. (iii) Printing/coating from particulate-based solutions. Electrodeposition is one of the well-established electrochemical techniques in the electronics industry.<sup>6</sup> However in this method, the deposition of multicomponent semiconductors like CIGSe is generally a complex process as the different elements have different redox potentials and reduction kinetics.<sup>7,8</sup> Multistep deposition might be necessary to provide a good control of stoichiometry and phase homogeneity. Among the approaches mentioned, the particulate- and precursor-based approaches have recently received a great deal of attention due to their potential to simplify the fabrication processing for large-scale manufacturing.

<sup>a</sup>Institute of Materials for Electronics and Energy Technology (I-MEET), Department of Materials Science and Engineering, Friedrich-Alexander University Erlangen-Nuremberg, Martensstrasse 7, 91058 Erlangen, Germany. E-mail: hamed.azimi@fau.de

<sup>b</sup>Bavarian Center for Applied Energy Research (ZAE Bayern), Haberstr. 2a, 91058 Erlangen, Germany

<sup>c</sup>Erlangen Graduate School in Advanced Optical Technologies (SAOT), Paul-Gordan-Str. 6, 91052 Erlangen, Germany



In this article, our main focus is dedicated to the solution-processed fabrication of chalcopyrite  $\text{CuInS}_2$  (CIS),  $\text{CuInSe}_2$  (CISE) and  $\text{Cu}(\text{In}, \text{Ga})(\text{Se}, \text{S})_2$  (CIGSSe) solar cells, addressing all the various methods like molecular, and particulate-based solutions as well as their hybrid combinations. Furthermore, as an important alternative to the CIGSSe technology, we also review the current state-of-the-art fabrication routes for solution processed kesterite  $\text{Cu}_2\text{ZnSnS}_4$  (CZTS),  $\text{Cu}_2\text{ZnSnSe}_4$  (CZTSe), and  $\text{Cu}_2\text{ZnSn}(\text{S}, \text{Se})_4$  (CZTSSe) solar cells.

## 2. Fundamental aspects of chalcopyrite and kesterite solar cells

### 2.1. Device concept

Fig. 2 shows a classical configuration of CIGSe and CZTSe solar cells, which is based on a heterojunction cell structure. The absorber layer with a thickness of typically 1–2  $\mu\text{m}$  is deposited

on molybdenum-coated soda-lime glass substrates. The heterojunction is then formed by the deposition of an n-type buffer layer (usually 50 nm CdS layer deposited by chemical bath deposition), the sputtering deposition of an intrinsic i-ZnO (typically with a thickness of 40–70 nm) and eventually of a transparent conductive oxide layer as the window layer (normally a heavily doped ZnO:Al or an indium-doped tin oxide (ITO) layer). A schematic band diagram of a CIGSe solar cell under zero-bias voltage condition is shown in Fig. 2. Some of the most critical recombination paths governing the diode current of such a solar cell structure are: recombination at the absorber surface, in the absorber bulk, at the absorber back contact, and in the absorber space charge region (SCR). The high probability for the charge carrier recombination at the absorber surface is one of the main disadvantages of such a cell structure; the advantage however is a negligible recombination in the buffer and window layer due to the large bandgap recombination in those regions. The high recombination at the heterojunction can be circumvented to a large extent by the proper design of the band diagram.<sup>10</sup> The highly doped CdS layer with a large bandgap of 2.4 eV is being typically used as an n-type layer in junction with a p-type CIGS or CZTS absorber layer in order to reduce the collection losses due to surface recombination (SR) of carriers photogenerated by short wavelength light and to transport electrons from the junction to the front surface. The recombination in the quasi-neutral region (QNR) largely depends on the bandgap gradients. The opportune bandgap gradient in chalcopyrite and kesterite solar cells can be achieved by controlled incorporation of Ga or S. Some examples of bandgap grading for solution processed chalcopyrite and kesterite solar cells are given in the following sections. The poor collection of carriers photogenerated at the back contact can be improved by enhancing the electron diffusion length ( $L_n$ ). A longer  $L_n$  can be achieved by passivating the interfaces, or increasing the crystallite size.<sup>11</sup>



*Hamed Azimi received his MEng in Electrical Engineering from Ferdowsi University of Mashhad, Iran. In December 2006, he joined Konarka Austria to study for a PhD under the supervision of Prof. Christoph. J. Brabec (Konarka) and Prof. Kurt Hingerl (Johannes Kepler University Linz, Austria). He obtained his PhD in Engineering Sciences in 2011. Since 2011, he has been a post-doctoral fellow in the group of*

*Prof. Brabec in the institute of Materials for Electronics and Energy Technology (i-MEET) at the Friedrich Alexander University Erlangen-Nürnberg, where he leads the group of solution processed inorganic and hybrid semiconductors for photovoltaic application.*



*Yi Hou is currently a PhD student under the supervision of Prof. Christoph J. Brabec at the institute of Materials for Electronics and Energy Technology (i-MEET) at Friedrich Alexander University Erlangen-Nürnberg (FAU). He received his MEng degree in Materials Science and Engineering from Beijing University of Chemical Technology (2012). He was awarded the Erlangen Graduate School in*

*Advanced Optical Technologies (SAOT) award in 2013. His research interest includes low-temperature solution processed inorganic and hybrid semiconductors and their applications in photovoltaics.*



*Christoph J. Brabec is holding the chair "Materials for Electronics and Energy Technology (i-MEET)" at the materials science department of the Friedrich Alexander University Erlangen-Nürnberg. Further, he is the scientific director of the Erlangen division of the Bavarian Research Institute for Renewable Energy (ZAE Bayern, Erlangen), board member of the ZAE Bavaria and board member*

*of the Energy Campus Nurnberg. Before joining the university, he was in SIEMENS research labs as the project leader for organic semiconductor devices and in Konarka Technologies Inc. as CTO. He is author and co-author of more than 200 papers and nearly 100 patents and patent applications.*



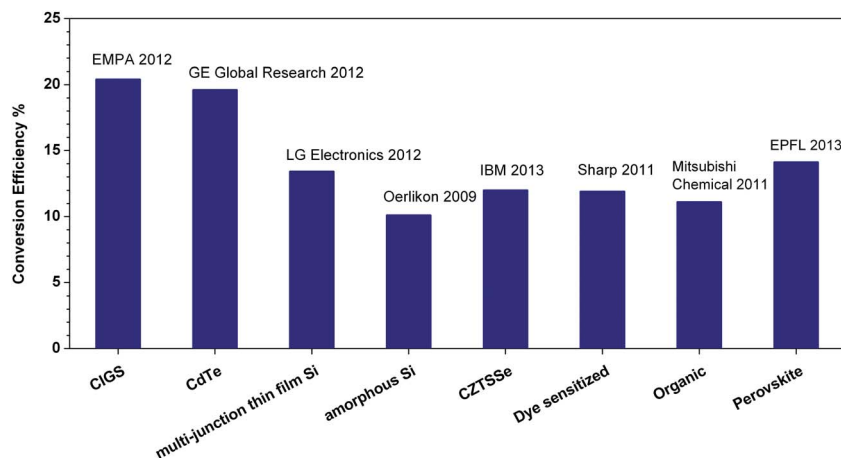


Fig. 1 Comparison between the world record efficiencies reported for various thin film solar cell technologies including for single cell and submodule devices. (Data extracted from the solar cell efficiency table reported by Green *et al.*<sup>9</sup>) Note: thin film GaAs and polycrystalline solar cells are not included in this comparison.

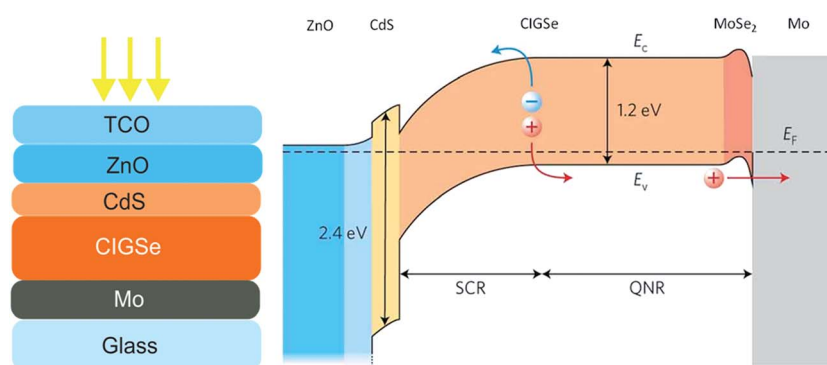


Fig. 2 Left – a schematic layer structure of a classical CIGSe solar cell. Right – a schematic band profile of a typical CIGSe solar cell under zero-bias voltage condition. The image of the band profile is reprinted with permission from ref. 12, Copyright 2011, Nature Publishing Group.

## 2.2. Grain boundaries and defects

In polycrystalline solar cells, the size of grains and the recombination velocity at the grain boundaries (GBs) are the key parameters to determine the rate of the charge carrier recombination. One primary influence of the GBs is the interruption of the long-range order in the crystal. A simple relationship between the effective diffusion length ( $L_{\text{eff}}$ ) for a polycrystalline material and a monocrystalline material can be defined as

$$L_{\text{eff}}^{\text{poly}} = \left[ (L_{\text{eff}}^{\text{mono}})^{-2} + 2S_g / (D_n g) \right]^{-1/2}, \quad (1)$$

where  $S_g$  stands for the recombination velocity at the grain boundaries of grains with the size  $g$  and  $D_n$  is the diffusion coefficient for electrons.<sup>13</sup> The GBs play an important role in controlling the current voltage characteristic of solar cells. The GBs may adversely influence the majority carrier mobility, therefore enhancing the series resistance. Also, the lifetime of the minority carriers can be reduced by increasing minority carrier recombination at GBs.<sup>11</sup> The GBs can even exhibit a recombination higher than in the bulk and additionally they

may become charged to induce band bending.<sup>10</sup> For examples, in high efficiency record CIGSSe devices, the loss in the open circuit voltage ( $V_{\text{oc}}$ ) is attributed to the electrostatic potential variations at charged extended defects like GBs.<sup>14</sup> There is however consensus that the GBs in chalcopyrites have more benign effects compared to other semiconductor materials.<sup>15</sup> The less negative influence of GBs is explained by multiple factors such as the inherently low GB recombination in CIGS, the beneficial effects of O and Na in the passivation of GBs and the reported downshift of the valence-band energy at GBs that effectively repels holes from the GB region.<sup>13,16–18</sup> The latter case is well attributed to the formation of a Cu-poor ordered defect compound (ODC) at the CIGS surface.<sup>19,16</sup> The effect of GBs is shown to be similarly benign in kesterites. However, studies showed that due to the constituent atoms at the GBs, more defect levels in the energy gap of CZTS bulk crystals can be found compared to CIGSe, which, in turn, enhance the probability of recombination of the photogenerated charge carriers.<sup>20</sup>

With respect to the different loss mechanisms discussed, it is important to understand the formation of the various defects



and secondary phases in chalcopyrites and kesterites. Defects may appear as single defect states with well defined energy levels within the bandgap or as multiple defect states and defect distributions with a quasi continuous state density in the bandgap.<sup>10</sup> In CIGSSe, the first-principle investigation showed that the indium-on-copper-antisites ( $\text{In}_{\text{Cu}}$ ) and the copper vacancy ( $V_{\text{Cu}}$ ) are, respectively, the dominant donor and acceptor defects.<sup>21,22</sup> The acceptor defect  $V_{\text{Cu}}$  is found to have a shallow ionization energy level and lower formation energy than the donor defects as  $\text{In}_{\text{Cu}}$  ( $\text{Ga}_{\text{Cu}}$ ) and  $\text{Cu}_i$ , explaining therefore the intrinsic p-type conductivity and also the difficulty in the control of n-type doping in this material. Furthermore in ternary chalcopyrites, due to the energetically favorable donor-acceptor compensation between  $V_{\text{Cu}}$  and  $\text{In}_{\text{Cu}}$ , there is a high probability of formation of defect clusters like  $[2V_{\text{Cu}} + \text{In}_{\text{Cu}}]$  and even the ordered defect compound such as  $\text{CuIn}_5\text{Se}_8$ .<sup>23</sup> In CZTS,  $V_{\text{Cu}}$  has similarly a low formation energy and becomes dominant in the case of Cu-poor and Zn-rich samples. Moreover, the cause of frequently observed non-stoichiometric kesterite samples can be explained on grounds of a strong tendency towards formation of self-compensated defect clusters, like  $[V_{\text{Cu}} + \text{Zn}_{\text{Cu}}]$ ,  $[\text{Zn}_{\text{Sn}} + 2\text{Zn}_{\text{Cu}}]$  and  $[2\text{Cu}_{\text{Zn}} + \text{Sn}_{\text{Zn}}]$ <sup>23,24</sup> (see Table 1 for a comparison between the dominant defects in chalcopyrites and kesterites).

For solution processed solar cells, the effects of grain boundaries and the defects can be very different from the devices fabricated based on the conventional vacuum deposition routes. The defect chemistry and the mechanisms of phase transformation can vary markedly depending on the initial solution precursors and the temperature used for the film deposition and the phase transformation. The losses induced by the smaller size of grains and the possible impurities from the precursors may exert a profound impact on the final device performance. To date, there have been very limited studies to provide in-depth insights into the properties and the loss mechanisms of solution processed chalcopyrite and kesterite devices. Fundamental insights using advanced characterization methods are still necessary to overcome the limitations in these devices.

### 2.3. Characterizations

Raman spectroscopy, X-ray diffraction, energy-/wavelength dispersive X-ray spectroscopy and X-ray fluorescence are

commonly being used to obtain information on crystalline quality, phase purity and chemical composition. Among the techniques mentioned above, Raman spectroscopy is an extremely useful technique that provides insight into the lattice strains and the existence and spatial distribution of different phases. Furthermore, in the preparation of molecular precursor solutions, Raman measurements can be used to analyze the degree of intermixing between the precursor components.<sup>25</sup> In CISSe samples, Raman spectroscopy can be used to distinguish the desired stable chalcopyrite (CH) from the metastable copper-gold CuAu (CA) and the metastable copper rich  $\text{CuIn}_5(\text{S}, \text{Se})_8$  structure.<sup>26–29</sup> For CZTS samples, while the coexistence of CZTS,  $\text{Cu}_2\text{SnS}_3$  (CTS), and ZnS may not be distinguishable by diffraction techniques, Raman analysis is able to detect and distinguish between these phases through their characteristic scattering peaks.<sup>30–33</sup> The employment of Raman spectroscopy at resonance conditions is shown to be essential for the distinction between the secondary phases in kesterites.<sup>34</sup> For a detailed overview on assignment of Raman peaks to different binary and ternary secondary phases related to the CZTS system, see ref. 30 and 34. To monitor the phase formation/transition during the thermal annealing, *in situ* techniques and thermal analyses like thermogravimetric analysis and differential thermal analysis are being implemented.<sup>35–38</sup>

To obtain information about the defect physics and their relationship to the device performance, characterization tools such as photoluminescence (PL),<sup>39–41</sup> admittance spectroscopy, deep level transient spectroscopy (DLTS)<sup>42–44</sup> and Hall measurements<sup>45,46</sup> are relevant. A combination of these techniques is generally necessary to analyze the shallow, mid-bandgap as well as the deep defects; while admittance measurements generally provide information on the deep defects, information on the density and the energy of shallow defects can be obtained by Hall and PL measurements.<sup>15</sup> In PL, studying the excitation intensity and the temperature dependence of the emission peaks sheds light onto the activation energies of the defects as well as the nature of the associated transitions.<sup>22,46</sup> At low temperatures and low excitation intensities, the PL spectrum can be dominated by the band-tail (BT) recombination. The BT recombination is the emission band that follows the band edge potential fluctuations originating from the local deviations in the distribution of donor and acceptor states (see Fig. 3). For instance, comparing the defect

**Table 1** Comparison of the bandgap, electrical conductivity and defect properties in the chalcopyrites and kesterites. Reprinted with permission from ref. 23, Copyright 2013, Wiley VCH

	$\text{CuInSe}_2$	$\text{CuGaSe}_2$	$\text{Cu}_2\text{ZnSnSe}_4$	$\text{Cu}_2\text{ZnSnS}_4$
Bandgap (eV)	1.04	1.68	1.0	1.5
Intrinsic conductivity	p-type	p-type	p-type	p-type
Hole-generating acceptors	$V_{\text{Cu}}^-$	$V_{\text{Cu}}^-$	$\text{Cu}_{\text{Zn}}^-, V_{\text{Cu}}^-$	$\text{Cu}_{\text{Zn}}^-, V_{\text{Cu}}^-$
High-population deep donors		$\text{Ga}_{\text{Cu}}^{2+}$		$\text{Sn}_{\text{Zn}}^{2+}, V_{\text{S}}^{2+}$
High-population clusters	$2V_{\text{Cu}} + \text{In}_{\text{Cu}}$	$2V_{\text{Cu}} + \text{Ga}_{\text{Cu}}$	$V_{\text{Cu}} + \text{Zn}_{\text{Cu}}$ $\text{Cu}_{\text{Zn}} + \text{Zn}_{\text{Cu}}$ $2\text{Cu}_{\text{Zn}} + \text{Sn}_{\text{Zn}}$ $\text{Zn}_{\text{Sn}} + 2\text{Zn}_{\text{Cu}}$	$V_{\text{Cu}} + \text{Zn}_{\text{Cu}}$ $\text{Cu}_{\text{Zn}} + \text{Zn}_{\text{Cu}}$ $2\text{Cu}_{\text{Zn}} + \text{Sn}_{\text{Zn}}$ $\text{Zn}_{\text{Sn}} + 2\text{Zn}_{\text{Cu}}$
Electron trapping clusters		$2V_{\text{Cu}} + \text{Ga}_{\text{Cu}}$		$2\text{Cu}_{\text{Zn}} + \text{Sn}_{\text{Zn}}$





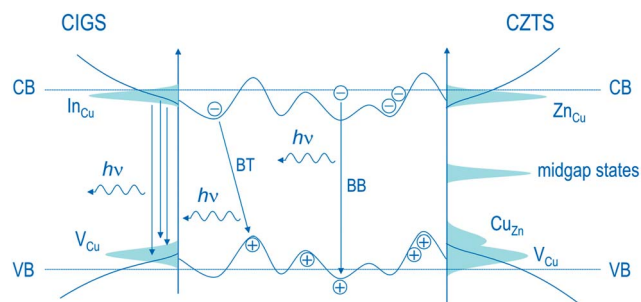


Fig. 3 Schematics of the band diagram for Cu-poor CIGSe and Cu-poor, Zn-rich CZTS, which represent the dominance of the band-tail (BT) and band-to-band (BB) transitions between delocalized donor and acceptor states. The energetic bands show potential fluctuations due to the local deviations in the distribution of donor and acceptor states. Reprinted with permission from ref. 22, Copyright 2011, American Physical Society.

properties of Cu-poor chalcopyrite and kesterite samples, a recent study found the higher probability of nonradiative recombination for the latter system. This conclusion was drawn on the basis of two observations: (1) the lower PL intensity and (2) the significantly high excitation densities needed for transition from a band-tail (BT) to a band-to-band (BB) recombination in CZTS. This result is consistent with the fact that kesterite has greater tendency towards formation of point defects with associated electronic states near the midgap.<sup>22</sup>

Another important method associated with PL spectroscopy is the time-resolved photoluminescence (TR-PL). TR-PL is used to directly measure the minority carrier lifetime in CIGSs and CZTSs devices.<sup>47,48</sup> The low minority carrier lifetime can result in higher dark current ( $J_0$ ) and can therefore promote the  $V_{oc}$  deficit in solar cell devices (eqn (2)).

$$V_{oc} = \frac{KT}{q} \ln\left(\frac{J_{sc}}{J_0} + 1\right), \quad (2)$$

Fig. 4 shows a TR-PL data of a 15.2% efficient hydrazine-based CIGSs solar cell.<sup>49</sup> A lifetime of  $\tau = 5.4 \pm 0.2$  ns was measured for this cell which is found to be lower than the lifetimes measured for high-performance vacuum-processed CIGSs solar cells ( $>10$  ns).<sup>48</sup>

To investigate the influence of GBs and their passivation on the performance of chalcopyrite and kesterite-based solar cells, scanning probe microscopy methods like scanning Kelvin probe microscopy (SKPM) and conductive probe atomic force microscopy (CP-AFM) are frequently used.<sup>50,51</sup> The simultaneous measurement of the surface film topography along with probing the variations of electrostatic surface potential (SKPM) and the current flow/surface conductivity (CP-AFM) at GBs documents important information with relevance to solar cell operation. High-resolution mapping can help in understanding whether the device performance is limited by grain bulk, grain surface, and/or GBs. A recent study,<sup>50</sup> comparing the surface potential maps of CIGSs, CZTS, and CZTSs, showed similarly for all the samples higher positive surface potentials at the GBs compared to the surface of the grains. This observation suggests that in

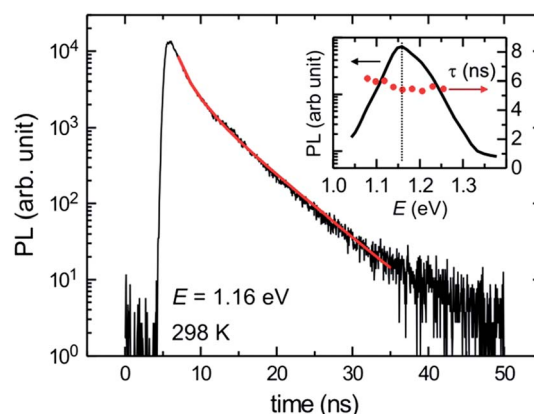


Fig. 4 Time-resolved photoluminescence (TR-PL) trace measured for the hydrazine-processed CIGSs with a PCE of 15.2%. Inset: the PL spectrum and the extracted lifetime in the vicinity of the band edge emission. Reprinted with permission from ref. 49, Copyright 2013, John Wiley & Sons, Ltd.

kesterites like CIGSs, GBs assist in the collection of minority carriers into the GBs. CP-AFM measurements were further used to demonstrate that there is no significant minority carrier recombination at GBs and the process of minority carrier collection by the GBs indeed occurs.

Besides the methods discussed above, a wide variety of other microscopic and spectroscopic techniques are available to study the electrical, optical, structural as well as the device properties of thin film solar cells (for a detailed overview, see ref. 52 and 53).

### 3. Solution processed chalcopyrite solar cells

#### 3.1. Deposition from molecular-based precursor solution

A solution based on a mixture of different molecular precursors can be directly used to produce films with a desired stoichiometric ratio of elements, high crystallinity and good uniformity in composition.<sup>54</sup> Chemical modifiers and sacrificial ligands are generally required to control the reaction kinetics and the solubility of precursor materials. Thermal treatment is being performed to convert the precursors into the desired phase and to remove the residual organic species. The concentration and the viscosity of the precursor solution are crucial factors impacting film formation and drying kinetics. Furthermore, the quality of the final metal chalcogenide film can be strongly influenced by the bulkiness and volatility of the sacrificial ligands. Small ligands are being preferred to avoid the formation of cracks and disruption of films during thermal decomposition.<sup>55</sup> Heat treatment at high temperatures in a sulphur or selenium atmosphere typically is necessary in order to complete the phase transformation and to minimize the porosity of the film.<sup>56</sup>

**3.1.1. Deposition from hydrazinium precursors.** The solution processability of metal chalcogenides is being limited by the presence of strong covalent bonds that result in poor



solubility in most solvents. A process known as dimensional reduction was successfully applied to overcome this limitation.<sup>57</sup> In this approach, addition of a strong ionic reagent breaks up the poorly soluble metal-anion framework. Sufficient incorporation of ionic reagents reduces the dimensionality of the framework substantially leading to the formation of oligomeric and monomeric components. The precursor solution containing metal chalcogenide anions reduced by cationic species is then used for film deposition. In the final step, the precursor film is being decomposed and transformed into the desired metal chalcogenide film upon heat treatment.<sup>57</sup> Hydrazine proved to be an excellent reducing agent for dissolving many different metal chalcogenides; it tends to strongly coordinate and has a small size and high vapor pressure that allows formation of the desired product with minimum impurities at relatively low temperatures. In recent years, this strategy was well established to fabricate high efficiency chalcopyrite (CIGSSe) and kesterite (CZTSSe) solar cells. Various metal sulfides and selenides, *e.g.*  $\text{Cu}_2\text{S}$ ,  $\text{In}_2\text{Se}_3$ ,  $\text{SnSe}$ ,  $\text{ZnS}$ , were efficiently dissolved in hydrazine to form soluble precursors. The disruption of the chalcogen framework in hydrazine was further significantly promoted by introducing elemental S and Se atoms.<sup>58,59</sup> Various deposition methods like spin-coating were applied to achieve the desired film thickness. After each deposition, an intermediate annealing step at  $250^\circ\text{C} \leq T \leq 350^\circ\text{C}$  is necessary to eliminate hydrazine and the extra S/Se. The final step requires annealing at temperatures above  $500^\circ\text{C}$  to promote grain growth and densification.<sup>60,61</sup> Mitzi *et al.*<sup>57,60,62</sup> developed the fabrication of CIGSSe solar cells using a hydrazine solution process, and reported recently a PCE of 15.2%,<sup>49</sup> which is one of the highest published device efficiencies among all solution-processed solar cells.

Despite the obvious superior performance of hydrazine-processed devices, the application of this process is limited by the toxicity and high reactivity of hydrazine. Recently, Zhou *et al.*<sup>63</sup> reported the use of non-hydrazine solutions for processing of  $\text{CuIn}(\text{S,Se})_2$  (CISSe) solar cells from hydrazinium precursors. The hydrazinium precursors were prepared by dissolving copper sulfide ( $\text{Cu}_2\text{S}$ ) and indium selenide ( $\text{In}_2\text{Se}_3$ ) precursors in hydrazine. The Cu-In hydrazinium precursors were found to be fairly soluble in a mixture of ethanolamine (EA) and dimethyl sulfoxide (DMSO). The solubility in the EA/

DMSO mixture is described by the reducing capability of EA and the tendency of the S atom in DMSO to coordinate with metal cores. The scheme in Fig. 5 illustrates the dissolution process for Cu-In hydrazinium into a solvent combination of EA/DMSO, where excessive S/Se is being added to accelerate the dissolution of precursors. The performance of solar cells fabricated by this approach was limited by the device thickness due to the lower degree of crystallinity and smaller grain size of films compared to the films from a pure hydrazine-based approach. Optimized CISSe solar cells fabricated using this method showed a device efficiency of 3.8% for an absorber film thickness of 300 nm, which is comparable to the hydrazine-based CISSe solar cells with a similar film thickness. Despite the apparent attractiveness, this technique still has the disadvantage of using hydrazine for preparation of initial precursors, which limits the applicability of the process.

**3.1.2. Non-hydrazine processing.** To evade the use of hydrazine, less toxic and environmentally benign solvents were employed to fabricate different chalcopyrite solar cells. A green formulation has been proposed based on the dissolution of different metal-nitrates and metal-halides in an alcoholic solvent.<sup>64</sup> Doctor blading a precursor paste prepared by dissolving an appropriate molar ratio of copper nitrate hemipentahydrate, indium chloride and gallium nitrate hydrate in methanol and a subsequent gas-phase selenization step yielded CIGSSe solar cells with an efficiency of 6.7%. The viscosity of the precursor solution for doctor blading was adjusted by adding a proper amount of ethyl-cellulose (EC). Ahn *et al.*<sup>54</sup> used a similar route based on the precursor solutions of  $\text{Cu}(\text{NO}_3)_2$  and  $\text{InCl}_3$  dissolved in methanol to produce  $\text{CuInSe}_2$  solar cells. The above synthesis route appeared to have the limitation induced by formation of a dense carbon layer between the absorber layer and the Mo back contact (Fig. 6). In an attempt to overcome this problem, the binder EC was replaced by polymethyl methacrylate (PMMA); although in this case no carbon-rich layer was observed, the performance of solar cells was limited by the film inhomogeneities and traces of parasitic oxide phases.<sup>65</sup> Following the approach described above, binder-free precursor solutions based on carboxylic chelate complexes and an alcoholic solvent have recently been used, leading to device efficiencies of up to 7.7%.<sup>66</sup> This process was based on an *in situ* oxidation of the organic solvent 1,2-propanediol and the coordination of carboxylic anions with metal species to form chelate complexes. Despite the efficiency improvement, the problem of a carbon-rich layer still remained due to the presence of carboxylate ligands. More recently, Park *et al.*<sup>67</sup> claimed almost carbon-free chalcopyrite  $\text{CuInGaS}_2$  solar cells with PCEs of over 8% based on a direct coating of a solution comprised of the nitrate salts of Cu, In and Ga and the additive polyvinyl acetate (PVA) as an organic binder. The phase transformation of a precursor film to the final chalcopyrite film was performed through an oxidation step followed by a sulfurization heat treatment process; the temperature for annealing was selected in such a way that removes the remaining materials from the binder.

Based on an alcoholic solution, acetate salts of the metals, namely, copper(II) acetate and indium(III) acetate, were also

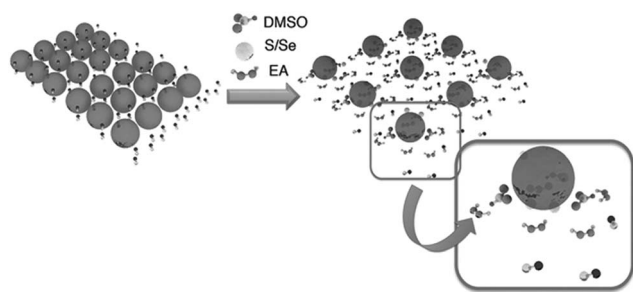


Fig. 5 Schematic representation of the dissolution mechanism for Cu-In hydrazinium in a solvent mixture of EA and DMSO. Reprinted with permission from ref. 63, Copyright 2012, Wiley VCH.



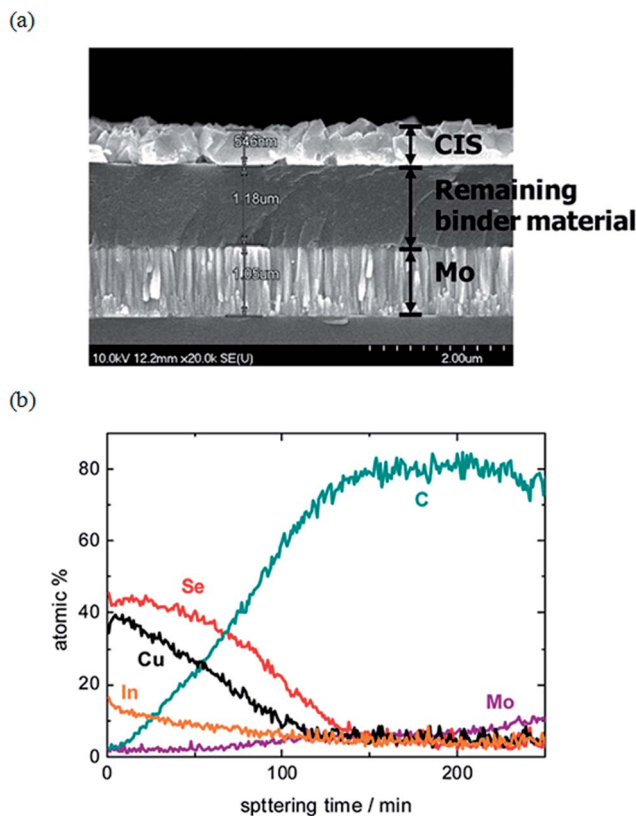


Fig. 6 (a) Cross-sectional SEM micrographs of a selenized film prepared based on a precursor solution comprised of metal-nitrates and metal-halides in methanol. (b) The corresponding Auger electron spectroscopy (AES) data depth profile of the selenized sample, confirming the presence of an amorphous carbon layer near the back Mo electrode. Reprinted with permission from ref. 54, Copyright 2010 American Chemical Society.

used to fabricate CIGSe solar cells.<sup>68,69</sup> For incorporation of gallium, the chloride or acetylacetonate (acac) salts of gallium were used. It was shown that a sufficiently high partial pressure of Se improves the grain size and the overall degree of crystallinity during the selenization process. Fig. 7 compares the SEM images of CIGSe films prepared by using different Se pressures, where high Se vapor pressure led to enhanced grain size and low carbon contamination. Compared to the different metal salts/alcohol-based routes discussed so far, the deposition from the

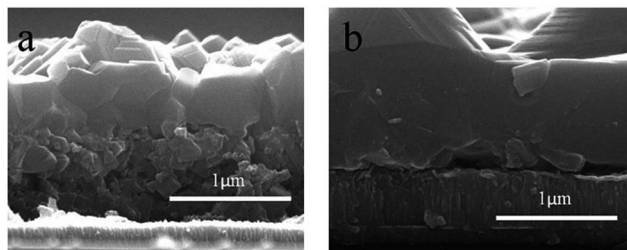


Fig. 7 (a) Cross-section SEM images of a CIGSe film grown with (a) low Se and (b) high Se vapor pressure. Reprinted with permission from ref. 69, Copyright 2012 Royal Society of Chemistry.

acetate salts/alcohol based precursor solutions has the important advantage of the possibility to form absorber layers with minimum carbon-residues. This is well demonstrated by Ahn *et al.*,<sup>70</sup> combining metal acetate salts with a mixture of ethanol and ethanolamine to fabricate 7.7% efficient CuInSe<sub>2</sub> solar cells with significantly lower levels of carbon impurity. Notably, the deposited CuInSe<sub>2</sub> films showed a low carbon content of <5 at %, already by a simple pretreatment in air at a temperature of 300 °C.

Cui and his group<sup>71</sup> introduced a process named as air stable ink rolling (AIR) to produce thin film CuInS<sub>2</sub> solar cells. This approach benefits from the use of rather low-cost precursors and an air-stable deposition method. The ink for CuInS<sub>2</sub> comprised of copper acetylacetonate (Cu(acac)<sub>2</sub>), indium acetylacetonate (In(acac)<sub>3</sub>) and elemental S dissolved in pyridine which is significantly less toxic compared to hydrazine. In this process, sulfur vulcanization with acetylacetonate provides the opportune viscosity and wetting properties for film processing. Films prepared by this approach were subsequently pre-baked at a temperature of 370 °C in air to burn off the organics and form a stack of Cu–In oxide layers. The precursor oxide films were then converted to CuInS<sub>2</sub> by a final sulfurization step in a bomb. The main deficiency of this approach was a poor control over the morphology and the film disruption induced during the sulfurization process resulting in solar cells with a low shunt resistance. Solar cells with PCEs of 2.15% were obtained after a post-KCN etching.

Apart from pyridine, other organic solvents with short ligands and strong coordinating properties were used to form an inexpensive and thermally degradable molecular precursor solution. For instance, a combination of butylamine and propionic acid was used to fabricate CuInS<sub>2</sub> nanocrystalline solar cells based on an *in situ* synthesis and film deposition route.<sup>72</sup> The attractive aspects of this approach are the simplicity of the process as well as a relatively low sintering temperature (<300 °C) used for the fabrication of solar cells. The drawbacks to this approach are however the poor stability of the precursor solution and a disordered film morphology.<sup>28</sup> Fig. 8 shows a scanning electron microscopy (SEM) image of a CuInS<sub>2</sub>

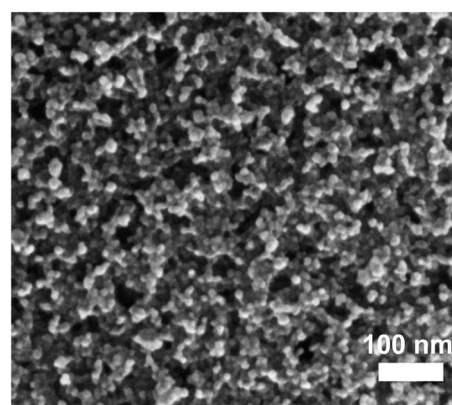


Fig. 8 (a) SEM top view image of a CuInS<sub>2</sub> NC film formed by an *in situ* deposition of precursor solution, sintered at a temperature of 270 °C. Reproduced with permission from ref. 28, Copyright 2013, Wiley VCH.







Fig. 9 (Top) Reaction mechanism of a metal oxide with butyldithiocarbamic acid. (Bottom) Digital photograph of various metal oxides dissolved in chloroform with the aid of butylamine and carbon disulfide ( $\sim 0.35$  M metal concentration). Reprinted with permission from ref. 73, Copyright 2012 American Chemical Society.

nanocrystal film prepared by the above approach. A detailed transport study of solar cells fabricated by this approach indicated a low carrier mobility of the CuInS<sub>2</sub> nanocrystal films, limiting the conversion efficiency to an absorber thickness smaller than 200 nm.<sup>28</sup> The use of an interpenetrating nanoscale heterojunction cell structure is expected to bypass the limitation of poor carrier collection at larger thicknesses.

Pan *et al.*<sup>73</sup> used a reaction of butylamine with carbon disulfide (CS<sub>2</sub>) to synthesize butyldithiocarbamic acid (BDCA) that could efficiently dissolve a number of different metal oxides. Fig. 9 shows the reaction mechanism of butylamine with CS<sub>2</sub> and the following reaction with a metal oxide, forming different thermally degradable metal-organic molecular precursor solutions. Solar cells fabricated by the selenization of films processed from a butyldithiocarbamic acid-based ethanol solution showed PCEs exceeding 10%,<sup>74</sup> which are currently the highest reported performances for hydrazine-free molecular precursor-based CIGSe solar cells. Furthermore, the nontoxic ink formulation and the stability of the precursor solution over the course of months underscore the importance of the work reported by Pan *et al.*

Another common approach to fabricate chalcopyrite solar cells is based on the spray deposition technique. Typically, an aqueous precursor solution containing chloride metal salts along with thiourea as the sulfur source, in the case of CuInS<sub>2</sub>,<sup>75–77</sup> and selenourea as the Se source, in the case of CuInSe<sub>2</sub>,<sup>78,79</sup> has been used. The deposition temperature is typically around 250–400 °C, which is a lower temperature compared to the temperatures used for sulfurization or selenization. One attractive application of spray deposition is to allow fabrication of three-dimensional (3D) nanocomposite cell structures. Based on a chemical spray deposition and incorporating the CuInS<sub>2</sub> nanocrystals into the matrix of In<sub>2</sub>S<sub>3</sub>/nanocrystalline anatase TiO<sub>2</sub>, Goossens *et al.*<sup>80</sup> reported solar cells with device efficiencies of about 5% (see Fig. 10).

A number of studies have reported the synthesis of single source organometallic precursors for deposition of ternary CuInS<sub>2</sub> and CuInSe<sub>2</sub> thin films.<sup>81–84</sup> Hirpo *et al.*<sup>81</sup> first described the synthesis of the compound (PPh<sub>3</sub>)<sub>2</sub>CuIn(SET)<sub>4</sub> to prepare the ternary CuInX<sub>2</sub> (X = S or Se) semiconductors. This compound comprises a copper(i) ion bound to two triphenylphosphine

ligands, an indium(III) ion with two terminal ethanethiolate ligands, and two ethanethiolate ligands coordinated between the metal centers.<sup>81,82</sup> The solubility of this compound in common organic solvents and the low decomposition temperature (<250 °C) make it an attractive candidate for spray pyrolysis deposition.<sup>81</sup> Banger *et al.*<sup>82–84</sup> have further developed the synthesis and deposition of single source precursors for ternary CuInX<sub>2</sub> semiconductors. Also, solar cells with an efficiency of 6.7% were reported using the single-source precursor of

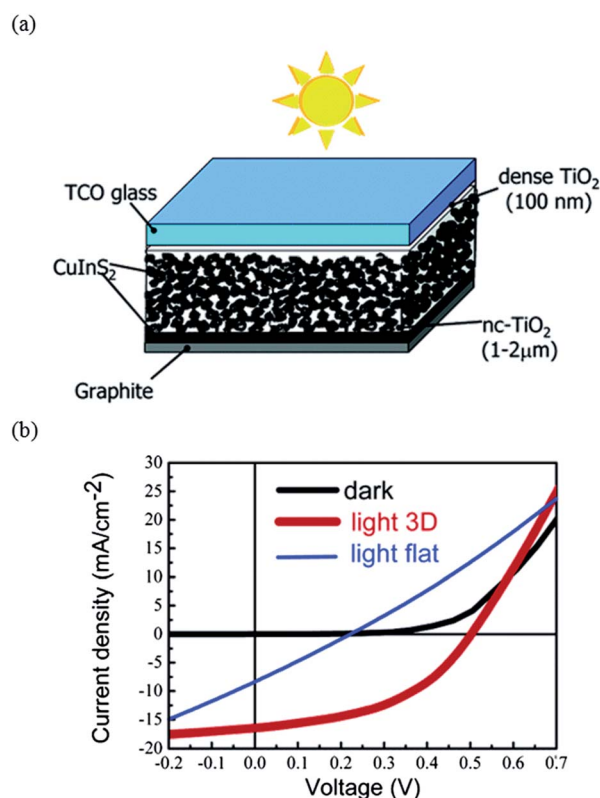


Fig. 10 (a) Schematic picture of a nanocomposite 3D solar cell, and (b) *J*–*V* characteristics of the 3D solar cell based on a TiO<sub>2</sub>/In<sub>2</sub>S<sub>3</sub>/CuInS<sub>2</sub> nanocomposite. Reprinted with permission from ref. 80, Copyright 2005, American Chemical Society.





Table 2 Non-exhaustive survey of chalcopyrite solar cells fabricated based on deposition from the molecular-based precursor solutions<sup>a</sup>

Year	Absorber	$J_{sc}$ (mA cm <sup>-2</sup> )	$V_{oc}$ (mV)	FF (%)	PCE (%)	Deposition and solvent	Post-treatment	Description	Ref.
2013	Cu(In,Ga)(S,Se) <sub>2</sub>	32.6	623	75	15.2	Spin-coating, hydrazine	540 °C (heat treatment under an inert atmosphere)	Hydrazinium precursors	49
2012	CuIn(S,Se) <sub>2</sub>	20.63	381	48.7	3.8	Spin-coating, EA/DMSO	400 °C (selenization)	Non-hydrazine solutions from hydrazinium precursors	63
2005	Cu(In,Ga)Se <sub>2</sub>	27.2	404	61	6.7	Doctor-blading, alcoholic solvent	550 °C (selenization in a Se/N <sub>2</sub> atm.)	Metal-nitrates and metal-halides	64
2013	CuInGaS <sub>2</sub>	17.0	787	61.9	8.28	Spin-coating, methanol	500 °C (sulfurization in a H <sub>2</sub> S/N <sub>2</sub> atm.)	Metal-nitrate salts	67
2011	CuIn <sub>x</sub> Ga <sub>1-x</sub> Se <sub>2</sub>	29.8	386	44	5.04	Inkjet-printing, ethanol, EG,* and EA	500 °C (selenization in a Se/H <sub>2</sub> /N <sub>2</sub> atm.)	Metal-acetate and chloride salts	68
2010	CuInS <sub>2</sub>	18.49	320	37	2.15	Ink-rolling, pyridine	525 °C (sulfurization in a bomb)	Metal-acetylacetonate salts, air-stable process	71
2010	CuInS <sub>2</sub>	12.38	588	54.8	3.99	Spin-coating, butylamine	250 °C (heat treatment under an inert atmosphere)	Indium acetate, copper iodide, and thiourea	72
2013	CuIn(S,Se) <sub>2</sub>	27.64	561	65.0	10.1	Spin coating ethanol with BDCA	540 °C (selenization in a Se atm.)	A mixture of metallic oxide NPs	74
2005	CuInS <sub>2</sub>	17	530	55	5	Spray-coating	Growth temperature 300 °C	Nanocomposite of TiO <sub>2</sub> /In <sub>2</sub> S <sub>3</sub> /CuInS <sub>2</sub>	80

<sup>a</sup> n.a. = Not available, \* ethylene glycol.

(PPh<sub>3</sub>)<sub>2</sub>CuIn(SET)<sub>4</sub> and based on an aerosol-assisted chemical vapor deposition.<sup>85</sup>

A brief summary of the reports discussed in this section, dealing with deposition from the molecular-based precursor solutions, is presented in Table 2.

### 3.2. Deposition from particulate-based solutions

In solution-based colloidal synthesis, it is possible to synthesize particles with a well-defined structure and high degree of purity. The nanoparticles offer a broad range of interesting tunable optical and electrical properties. Moreover, they offer excellent solution processing and their high reactivity is advantageous for phase transformation and film densification.<sup>86,87</sup> In the synthesis of nanoparticles, it is very important to form particles with a uniform size and composition and with low levels of structural disorder. The use of organic ligands is generally required to properly control the kinetics of nucleation and growth during the synthesis. The organic ligands also play a key role in providing colloidal stability and later in assembling individual particles into a nanocrystal solid.<sup>88</sup> The common organic surfactants are the long chain alkyl ligands like trioctylphosphite and oleylamine.<sup>89–91</sup> Due to the insulating properties of these ligands that hamper an efficient transport between the nanoparticles, a complete removal of the organic ligands is crucial. The need for removal of bulky organic ligands can however result in generation of cracks and discontinuities in the nanoparticle film and may leave behind unwanted carbonaceous impurities and surface defects.<sup>55</sup> To overcome the above issues, additional processing steps like ligand-exchange, heat treatment or chemical treatment are usually necessary.<sup>90,92–94</sup>

In this section, we review the most recent work employing colloidal nanoparticle solutions for fabricating CIGS and

chalcopyrite-based thin film solar cells. Table 3 presents a summary of some selected results along with information for the corresponding device parameters and preparation details. The section is sub-categorized into the use of (a) single phase, (b) binary or multi-phase particles as starting precursors for the film deposition. The discussion on the chemistry and properties of inorganic nanoparticles is not the purpose of this review. For detailed information, the reader is urged to refer to the number of excellent reviews that comprehensively address the mechanism of growth and the properties of inorganic nanoparticles.<sup>95–97</sup>

#### 3.2.1. Ternary and quaternary phase nanoparticles.

Controlling the phase transition of a nanoparticulate film into a desired bulk composite is one of the most challenging aspects of device fabrication. This is particularly difficult when it comes to the direct use of pure ternary or quaternary nanoparticles. Despite many studies reporting the synthesis of single chalcopyrite CIS, CISE, CIGS and CIGSe particles,<sup>55,98–100</sup> the direct use of them to fabricate efficient solar cell devices has rarely been reported. One problem is that single phase nanoparticles can be decomposed to different binary phases or to their pure metal constituents during the sintering process. Another difficulty is the frequently higher melting temperature of ternary or quaternary particles compared to their binary phase particles; this may hinder an effective sintering of nanoparticles during crystallization.

One of the first reports on the use of colloidal nanoparticles in solar cells was by Guo *et al.*,<sup>101</sup> reporting solar cells with a PCE of 3.2% based on a CuInSe<sub>2</sub> nanoparticle ink. Oleylamine was used as the capping agent during the synthesis and nanoparticles were dispersed in toluene. The nanocrystals were successfully sintered to micrometer large crystalline grains



Table 3 Non-exhaustive survey of chalcopyrite solar cells fabricated based on deposition from the particulate-based solutions<sup>a</sup>

Year	Absorber	$J_{sc}$ ( $\text{mA cm}^{-2}$ )	$V_{oc}$ (mV)	FF (%)	PCE (%)	Deposition and solvent	Post-treatment	Description	Ref.
2008	CuInSe <sub>2</sub>	25.8	280	39	2.82	Drop-casting	450–550 °C (selenization in a Se/Ar atmosphere)	CuInSe <sub>2</sub> NPs (CuCl, InCl <sub>3</sub> and Se in OLA)	101
2009	Cu(In <sub>1-x</sub> Ga <sub>x</sub> )(S <sub>1-y</sub> Se <sub>y</sub> ) <sub>2</sub>	23.7	455	51.5	5.5	Drop-casting, toluene	500 °C (selenization in a graphite box)	Cu(In <sub>1-x</sub> Ga <sub>x</sub> )S <sub>2</sub> NPs (metal-chlorides and S in OLA)	90
2013	Cu(In,Ga)(S,Se) <sub>2</sub>	28.8	630	65.7	12	Doctor-blading, hexanethiol	500 °C (selenization in a graphite box)	Cu(In <sub>1-x</sub> Ga <sub>x</sub> )S <sub>2</sub> NPs (metal(acac) salts and S in OLA)	102
2010	CuInSe <sub>2</sub>	16.3	410	46	3.1	Spray-coating	n.a.	CuInSe <sub>2</sub> NPs (metal-chlorides and Se in a mixture of OLA and TBP)	104
2000	CuInSe <sub>2</sub>	37.5	430	65.5	10.56	Spray-coating, aqueous dispersion	440 °C (selenization in a H <sub>2</sub> Se/N <sub>2</sub> atm.)	Sub-micron sized Cu–In alloy particles (melt atomization technique)	111
2003	CuIn <sub>1-x</sub> Ga <sub>x</sub> Se <sub>2</sub>	37.3	520	71	13.6	Printing	420–450 °C (reduction and selenization in H <sub>2</sub> /N <sub>2</sub> and H <sub>2</sub> Se/N <sub>2</sub> gas)	A mixture of oxide NPs (chemical approach)	113
2011	CuInSe <sub>2</sub>	34.3	352	57	7.0	Doctor-blading	550 °C (selenization in a Se/N <sub>2</sub> atm.)	Citrate-capped Cu <sub>11</sub> In <sub>9</sub> NPs (NaBH <sub>4</sub> -assisted chemical reduction)	86
2012	CuInSe <sub>2</sub>	33.7	440	55	8.2	Drop-casting	530 °C (selenization)	NPs of CuInSe <sub>2</sub> , CuSe, Cu <sub>2-x</sub> Se, and In <sub>2</sub> O <sub>3</sub> (microwave-assisted synthesis)	119

<sup>a</sup> n.a. = Not available., NPs = nanoparticles, OLA = oleylamine, TBP = tributylphosphine.

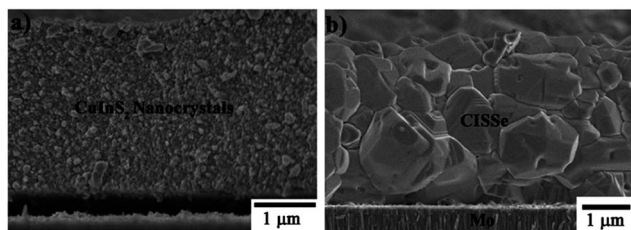


Fig. 11 FE-SEM images of (a) CuInS<sub>2</sub> nanocrystal film prepared on a Mo-coated soda lime glass substrate by drop-casting of nanocrystal ink and (b) after selenization at 500 °C for 45 min showing the formation of large crystalline grains and high compactness of the film. Reprinted with permission from ref. 90, Copyright 2009 American Chemical Society.

through an annealing step at temperatures of 450–550 °C under Se vapor. To remove the organic capping molecules prior to selenization, films were annealed under a flow of argon gas at 500 °C. The selenization however caused the inclusions of void space in the absorber film, imposing a major constraint on the photovoltaic performance. One year later and based on the same synthesis approach, Guo *et al.* improved the efficiencies to over 5% using sulfur based nanoparticulate inks, *i.e.* CuInS<sub>2</sub> and Cu(In<sub>1-x</sub>Ga<sub>x</sub>)S<sub>2</sub> instead of CuInSe<sub>2</sub>. This exchange significantly promoted the volume expansion during the selenization process and led to the formation of a denser absorber film (see Fig. 11).<sup>90</sup> Quaternary CIGS nanoparticles were designed instead of ternary sulfide and selenide nanoparticles to facilitate band-gap engineering. Most recently, hexanethiol based ink in combination with NaCl treatment yielded a 12% efficient

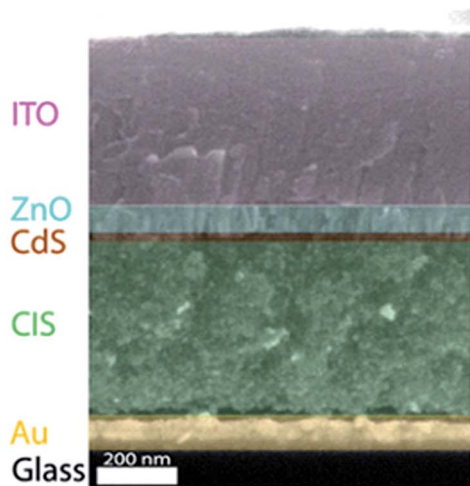
Cu(In,Ga)(S,Se)<sub>2</sub> nanocrystal-based solar cell.<sup>102</sup> The positive influence of Na inclusion was attributed to an improved microstructure, substantially reducing recombination losses.

As mentioned above, post-thermal selenization poses additional costs and technological impediments on the production process. From this standpoint, it is important to highlight the work by Korgel *et al.*,<sup>103</sup> reporting colloidal CuInSe<sub>2</sub> nanoparticle based solar cells without high temperature sintering. By spray-depositing CISE and CIGSe nanoparticles and by optimizing the device structure, solar cells with PCEs of up to 3.1% were reported (see Fig. 12).<sup>104,105</sup> In this study, the conventional Mo back contact was replaced by gold (Au) to ensure a good ohmic contact to the absorber layer. The general consensus is that a thin layer of MoSe<sub>2</sub>, which is being formed during the crystallization process at high temperatures, subjects Mo to a selective electrical contact for CISE and CIGSe absorber layers.<sup>106,107</sup>

The strategy to design new capping agents is an attractive way to improve the performance of nanocrystal-based solar cells without high temperature processing. All the experiments mentioned above have focused on the use of oleylamine as the capping agent. In attempting to improve the transport properties and functionality of nanoparticle based solar cells, different inorganic moieties including inorganic metal chalcogenide-hydrazinium complexes (MCC), S<sup>2-</sup>, HS<sup>-</sup>, and OH<sup>-</sup> were adopted.<sup>89</sup> However, no improvement over the oleylamine-capped nanoparticles was found for MCC-capped CISE nanoparticles, which in addition had the drawback of using toxic and highly reactive hydrazine. The above study nevertheless showed that further studies on understanding and the engineering of novel ligands can facilitate low-temperature processed nanocrystal-based solar cells with high performance.



(a)



(b)

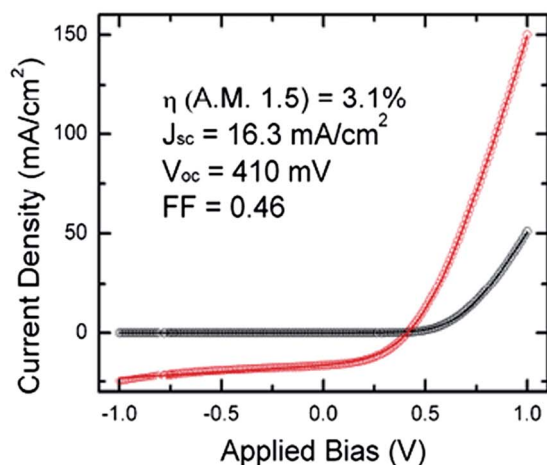


Fig. 12 (a) Cross-sectional SEM picture of a solar cell fabricated by spray-depositing of  $\text{CuInSe}_2$  nanoparticles without the use of any high temperature processing (reprinted with permission from ref. 105, Copyright 2012 Elsevier B.V.) and (b) the corresponding current–voltage characteristics measured under  $100 \text{ mW cm}^{-2}$  AM1.5G (reprinted with permission from ref. 104, Copyright 2010 Optical Society of America).

**3.2.2. Binary and multinary phase nanoparticles.** Different colloidal nanoparticle precursors including elemental metals, metallic alloys, binary metal chalcogenides and metal oxide nanoparticles can be used to form chalcopyrite thin films. A typically lower melting temperature ( $T_m$ ) and higher reactivity of such nanoparticles as compared to the ternary or quaternary particles can ease the process of phase transformation and film densification. Studies on this approach were first focused on preparing powders of micro- and submicron-sized particles, and then dispersing them in a proper liquid media. Top-down techniques like milling and grinding techniques were often used for the particle size reduction.<sup>108–110</sup> In one of the previous reports, Arita *et al.*<sup>108</sup> described the preparation of a screen

printing paste using ball-milled Cu, In and amorphous Se powders mixed with ethylene glycol monophenyl ether as the binding agent. The neat  $\text{CuInSe}_2$  phase was formed after a sintering process at high temperatures of  $700^\circ\text{C}$  in a  $\text{N}_2$  atmosphere. The process was further improved by coating intermetallic Cu–In particles with a subsequent selenization process. Basol *et al.*<sup>109</sup> and Norsworthy *et al.*<sup>111</sup> reported solar cells with efficiencies of up to 10% using sub-micron sized Cu–In alloy particles prepared by a melt atomization technique. The as-deposited precursor layers comprised of  $\text{Cu}_{11}\text{In}_9$  and  $\text{CuIn}_2$  particles were selenized in the presence of  $\text{H}_2\text{Se}$  to obtain a dense chalcopyrite  $\text{CuInSe}_2$  film. Most recently, a process involving metallic particles of Cu, In and Ga in combination with subsequent selenization allowed the fabrication of  $\text{CuIn}_{1-x}\text{Ga}_x\text{Se}_2$  devices with PCE of over 7%.<sup>112</sup>

As the line of research continued, a significant portion of the research was devoted to the preparation of particles *via* chemical means. Kapur *et al.*<sup>113</sup> obtained high efficiency devices with PCEs exceeding 13% using a mixture of oxide based nanoparticles, which were reduced and selenized in  $\text{H}_2/\text{N}_2$  and  $\text{H}_2\text{Se}/\text{N}_2$  gas. The intermetallic Cu–In particles were also synthesized through a chemical reduction method.<sup>114–117</sup> The inorganic compound sodium borohydride ( $\text{NaBH}_4$ ) was commonly used as the reducing agent.  $\text{NaBH}_4$  is a mild and inexpensive reagent whose reactivity is enhanced in the presence of certain organic and inorganic compounds.<sup>118</sup> However, efforts to fabricate solar cells based on  $\text{NaBH}_4$ -assisted chemical reduction led to fairly low efficiency devices ( $\leq 1.4\%$ ). The problem was mainly related to the high level of porosity and structural free volume in the films.<sup>114,116</sup> The breakthrough in this approach was reported by Kind *et al.*,<sup>86</sup> demonstrating 7% efficient solar cells based on the deposition of citrate-capped  $\text{Cu}_{11}\text{In}_9$  nanoparticles, followed by selenization under  $\text{H}_2\text{Se}$ . The  $\text{Cu}_{11}\text{In}_9$  particles with a diameter of 10–30 nm were prepared by a polyol-mediated synthesis, where an aqueous solution of  $\text{NaBH}_4$  was injected into a solution of  $\text{CuCl}_2$ ,  $\text{InCl}_3$ , and disodium citrate hydrate in diethylene glycol (see Fig. 13 for the electron microscopy image of as-prepared nanoparticles). The role of disodium citrate was not only to control the nucleation and stability of the  $\text{Cu}_{11}\text{In}_9$  nanoparticles, but also to effectively suppress the particle-to-particle agglomeration. Recently, organic free Cu–In alloy nanoparticle precursor ink was prepared by  $\text{NaBH}_4$ -assisted chemical reduction and used to fabricate a  $\text{CuInSe}_2$  absorber layer, but only solar cells with a low PCE of 3.92% were reported.<sup>87</sup>

Another interesting approach was reported by Jeong *et al.*,<sup>119</sup> who used a mixture of nanoparticles of  $\text{CuInSe}_2$ ,  $\text{CuSe}$ ,  $\text{Cu}_{2-x}\text{Se}$ , and  $\text{In}_2\text{O}_3$  to fabricate  $\text{CuInSe}_2$  devices with efficiencies of up to 8.2%. The multiphase nanoparticles in this study were produced *via* a microwave-assisted solvothermal synthesis. In microwave processing, due to the tendency of particles to precipitate in a fast and nearly simultaneous manner, the synthesis of particles with small size and narrow size distribution is possible.<sup>95</sup>

Another interesting concept was introduced by Min Lim *et al.*,<sup>120</sup> reporting the formation of quaternary  $\text{CuInS}_3\text{Se}_{1-x}$  nanoparticles *via* chemical welding of binary  $\text{CuSe}$  and  $\text{In}_2\text{Se}_3$  nanoparticles at room temperature. Contrary to most reports,





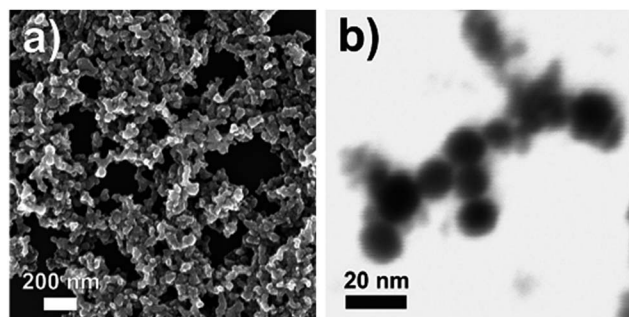


Fig. 13 Electron microscopy of citrate-capped  $\text{Cu}_{11}\text{In}_9$  nanoparticles: (a) SEM overview image, and (b) detailed bright-field STEM image. Reprinted with permission from ref. 86, Copyright 2011 American Chemical Society.

the coalescence and sintering of particles were performed in the liquid phase, and imposed by oppositely charging the CuS and  $\text{In}_2\text{S}_3$  nanoparticles (schematically outlined in Fig. 14). To establish opposite charges on the particle surface, the nanoparticles were synthesized in the presence of polyacrylic acid (PAA) and polydiallyldimethylammoniumchloride (PDAA), respectively, for CuS and  $\text{In}_2\text{S}_3$  nanoparticles.

Most of the studies discussed so far employed relatively crystalline nanoparticles. Nevertheless, due to the high melting temperature of crystalline particles, they might not be necessarily the best choice for device fabrication. Ahn *et al.*<sup>121,122</sup> reported the synthesis and utilization of amorphous Cu–In–Se nanoparticles, aiming to benefit from the lower melting temperatures of such particles to assist an effective sintering during a post-thermal treatment.  $\text{CuInSe}_2$  films formed from amorphous Cu–In–Se nanoparticles showed dense morphologies for particles modified by chelate complexation with ethanolamine. Recently, they demonstrated devices with efficiencies of up to 7.9% from modified amorphous nanoparticles.<sup>123</sup>

### 3.3. Deposition from nanoparticles/precursor solution

Hybrid inks are interesting from the perspective of combining the advantages of particulate-based and molecular-based

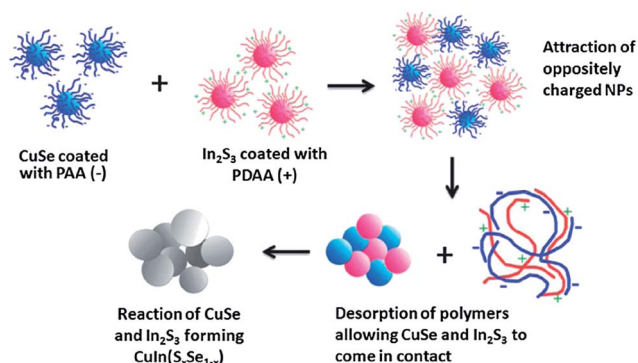


Fig. 14 A schematic diagram representing the formation of  $\text{CuInS}_x\text{Se}_{1-x}$  nanoparticles through electrostatically induced coalescence and sintering of binary CuSe and  $\text{In}_2\text{Se}_3$  nanoparticles. Reprinted with permission from ref. 120, Copyright 2013, The Royal Society of Chemistry.

precursor solutions. In a hybrid ink of nanoparticles mixed into a precursor, the precursor solution can be used as a medium to provide effective binding between nanoparticles. Further, the particles can act as nucleation sites to promote grain growth and film densification. Cho *et al.*<sup>124</sup> developed a hybrid ink using a mixture of colloidal CuS nanoparticles and an indium precursor solution to form a dense layer of  $\text{CuInSe}_2$ , demonstrating solar cells with efficiencies of over 6% after selenization. Similar device efficiencies were reported by Cai and coworkers based on spray deposition from a hybrid ink containing molecular precursors of  $\text{CuCl}_2$ ,  $\text{InCl}_3$ , and thiourea mixed with CuS and  $\text{In}_2\text{S}_3$  nanoparticles.<sup>125</sup> The inclusion of CuS and  $\text{In}_2\text{S}_3$  nanoparticles in the precursor solution led to a substantial improvement in device performance, mainly as a result of increased  $J_{\text{sc}}$  and  $V_{\text{oc}}$ . The comparison between the  $J$ – $V$  characteristics of devices made from a precursor solution and a nanoparticle/precursor solution is shown in Fig. 15.

### 3.4. Hybrid organic/inorganic solar cells

Inorganic semiconductor nanocrystals were investigated in combination with organic molecules or nanostructure metal oxides to combine attractive features of both classes of materials for applications like photodetectors and photovoltaics.<sup>126–128</sup> Because of the high carrier mobility and tunable absorption properties, inorganic NCs are attractive to be used as electron accepting or donating materials for organic solar cells. These attractive features can be beneficial when combined with the low temperature processing of organic solar cells.<sup>129</sup>

$\text{CuInS}_2$  and  $\text{CuInSe}_2$  nanoparticles were used as electron acceptors<sup>130,131</sup> or electron donors<sup>132</sup> in combination with different polymers or organic small molecules to form a bulk-heterojunction solar cell structure. The semiconducting properties of  $\text{CuInS}_2$  can be modified, depending on the ratio between Cu and In, to a p-type ( $\text{Cu}/\text{In} > 1$ ) or an n-type ( $\text{Cu}/\text{In} < 1$ ) semiconductor.<sup>133</sup>

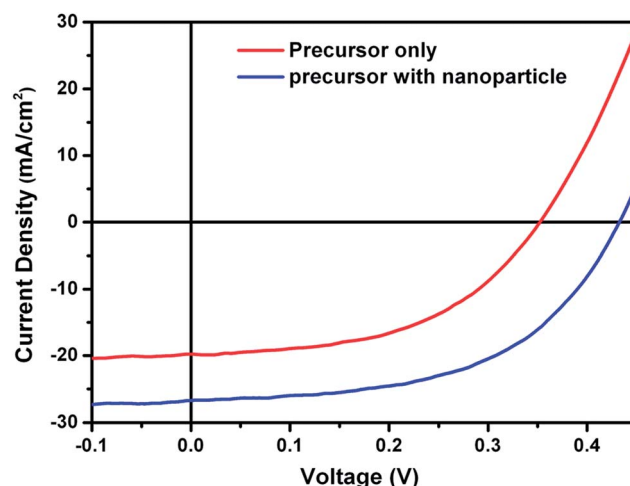


Fig. 15  $J$ – $V$  curve of the device fabricated from a nanoparticle incorporated precursor film (blue) and a precursor film without nanoparticles (red). Reprinted with permission from ref. 125, Copyright 2013 American Chemical Society.





In a blend of colloidal CuInS<sub>2</sub> nanoparticles with conjugated polymers, the process of charge transfer was observed by photoluminescence and photo-induced absorption spectroscopic measurements.<sup>134,135</sup> However, due to the limitations imposed by the presence of organic ligands as well as surface traps on the nanoparticles, fairly low efficiencies were reported (PCEs < 1%).<sup>132,134–136</sup> The intricacy of controlling the morphology is another decisive factor, influencing the performance of hybrid solar cells. Such issues could be largely overcome by an *in situ* formation of the inorganic nanocrystals directly inside an organic matrix. This approach has the advantages of eliminating the need for a separate nanoparticle synthesis and the use of an organic capping ligand.<sup>137,138</sup> The *in situ* formation of CuInS<sub>2</sub> nanoparticles in an organic semiconductor was described by Rath *et al.*<sup>139</sup> and Maier *et al.*<sup>131</sup> The process reported by Rath *et al.* is schematically described in Fig. 16, in which the CuInS<sub>2</sub> nanoparticles were directly formed in the matrix of the conjugated polymer, poly[(2,7-silafluorene)-alt-(4,7-di-2-thienyl-2,1,3-benzothiadiazole)] (PSiF-DBT), using easily thermally decomposable organometallic complexes, copper xanthates and indium xanthates. A mild annealing step at 200 °C was used to complete the fabrication of nanocomposite CuInS<sub>2</sub>/PSiF-DBT solar cells. A conversion efficiency of 2.8% was achieved, which is one of the highest efficiencies ever reported for polymer/CIS nanocomposite solar cells.

A summary of the solar cell results associated with the use of hybrid mixtures, *i.e.* nanoparticles/precursor and inorganic/organic, is given in Table 4.

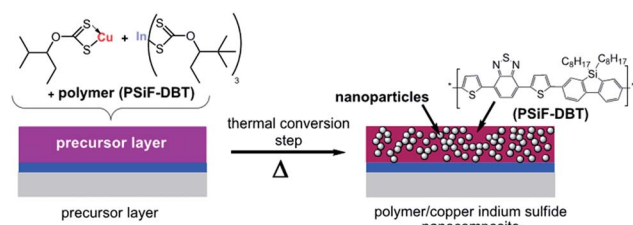


Fig. 16 Schematic representation of the polymer/CIS nanocomposite formation. Reprinted with permission from ref. 139, Copyright 2011, Wiley VCH.

## 4. Solution processed kesterite solar cells

Kesterite-based compounds, *i.e.* Cu<sub>2</sub>ZnSnS<sub>4</sub> (CZTS), Cu<sub>2</sub>ZnSnSe<sub>4</sub> (CZTSe), and Cu<sub>2</sub>ZnSn(S,Se)<sub>4</sub> (CZTSSe), are materials showing optical and electronic properties comparable to those of the chalcopyrite CuInS<sub>2</sub>, CuInSe<sub>2</sub> and Cu(In, Ga)(Se, S)<sub>2</sub> materials, however with the advantage of being composed of only abundant and economical elements.<sup>31</sup> Among all, CZTS with an optimal bandgap of 1.5 eV and a large absorption coefficient of 10<sup>4</sup> cm<sup>-1</sup> is one of the best absorber materials for solar cell mass production.<sup>140</sup> Despite the promising potential, there is still a significant performance gap between the best kesterite-based and chalcopyrite solar cells (see Fig. 1). The reason can be found in manifold complexities related to the crystal structure, stoichiometry, point defects and morphology of kesterite. Due to the narrower existence region of the kesterite phase compared to the analogous chalcopyrites, secondary phases and point defects are a serious challenge in this material system.<sup>23,141</sup> Fig. 17 compares the calculated stable chemical potential range for chalcopyrite CuInSe<sub>2</sub> and kesterite Cu<sub>2</sub>ZnSnS<sub>4</sub>, showing the more complicated limit to the chemical potential region for the latter compound.

In order to close the performance gap with CIGSSe, further applied and theoretical studies are necessary to understand the underlying interfaces and corresponding defects of the CZTSSe system. Interestingly, the presently highest efficiency CZTSSe devices are based on fabrication *via* solution-processing methods. One of the major issues is the more volatile mix of elements (*e.g.* Sn) in the CZTSSe system, causing a severe limitation for the vacuum based techniques requiring post-thermal treatment at temperatures >400 °C.<sup>142,143</sup> Although this problem is largely resolved by heat treatments under different chalcogen-containing (*e.g.* Sn) atmospheres,<sup>144</sup> the device efficiencies are still below those prepared by liquid-based processing.

### 4.1. Hydrazine solution processing of CZTS(e)

Currently, there are two types of hydrazine based solution processing routes: one is based on a hybrid mixture of nanoparticles and a precursor solution, which involves undissolved

Table 4 Survey of chalcopyrite solar cells fabricated based on deposition from the nanoparticles/precursor solutions and summary of hybrid chalcopyrite nanoparticles/polymer solar cells<sup>a</sup>

Year	Absorber	$J_{sc}$ (mA cm <sup>-2</sup> )	$V_{oc}$ (mV)	FF (%)	PCE (%)	Deposition and solvent	Post-treatment	Description	Ref.
NPs/precursor	CuInSe <sub>2</sub>	31.01	420	47.5	6.23	Spin-coating	530 °C (selenization)	CuS NPs and an indium precursor solution	124
NPs/precursor	CuIn(S,Se) <sub>2</sub>	26.7	430	53	6.15	Spray-coating	480–500 °C (selenization)	Molecular precursors of CuCl <sub>2</sub> , InCl <sub>3</sub> , and thiourea mixed with CuS and In <sub>2</sub> S <sub>3</sub> NPs	125
Hybrid inorganic/organic	P3HT*/CuInSe <sub>2</sub>	0.56	440	30	0.7	Spin-coating	Annealing at 220 °C	CuInSe <sub>2</sub> nanocrystals mixed with P3HT weight ratio of 1 : 6	135
Hybrid inorganic/organic	CuInS <sub>2</sub> /PSiF-DBT	10.3	540	50	2.8	Spin-coating	Annealing at 200 °C	<i>In situ</i> formation of CuInS <sub>2</sub> NPs in polymer	139

<sup>a</sup> NPs = nanoparticles.



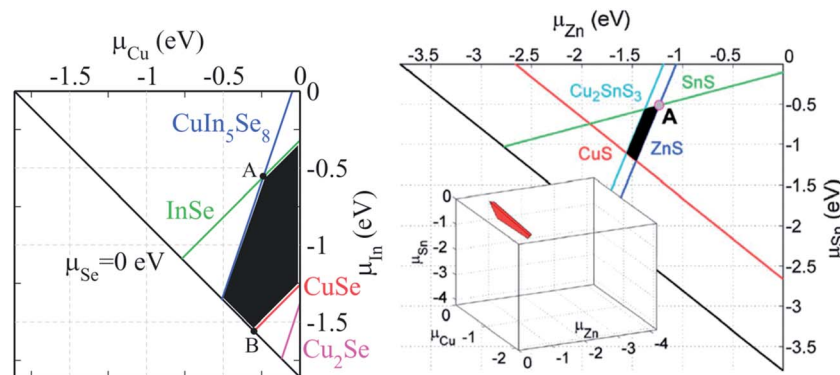


Fig. 17 The calculated chemical potential diagram of (left)  $\text{CuInSe}_2$  in the  $(\mu_{\text{Cu}}, \mu_{\text{In}})$  plane and (right)  $\text{Cu}_2\text{ZnSnS}_4$  in a 2D Cu-rich plane (the stable 3D region is shown in the inset).<sup>24</sup> The black area shows the chemical potentials under which  $\text{CuInSe}_2$  and  $\text{Cu}_2\text{ZnSnS}_4$  are thermodynamically stable against different competing secondary compounds. Reprinted with permission from ref. 31 and 23, Copyright 2012 and 2013, Wiley VCH.

Zn particles and truly dissolved precursor solutions,<sup>145</sup> and another is a purely molecular based approach which involves all the chalcogenides fully dissolved at a molecular level.<sup>146</sup> Both of these approaches exhibited highly efficient solar cells. Originating from the previous works on hydrazine processed CIGSSe absorbers, Mitzi *et al.*<sup>145</sup> demonstrated the fabrication of CZTSSe thin film solar cells with 11.1% power conversion efficiency using a hydrazine-based hybrid approach. Quite recently, by optimizing the thickness of the CdS and transparent-conducting layers, Mitzi *et al.* improved the device efficiency to 12.0%.<sup>147</sup> Until today, this performance holds the highest reported efficiency for this material system. Another hydrazine-based approach was reported recently by Yang *et al.*<sup>146</sup> In this study, the hydrazine derivatives were designed to allow the effective incorporation of zinc compounds into hydrazine solution, forming a CZTS precursor solution that is homogeneous at the molecular level. Based on a deposition from this precursor solution and a subsequent selenization process, a solar cell with an efficiency of 8.08% was produced.

#### 4.2. Non-hydrazine solution processing of CZTS(e)

Although among all available fabrication routes including both vacuum and non-vacuum based techniques, the hydrazine based approach has yielded the highest efficiency kesterite solar cells, as previously mentioned, the explosivity and toxicity of hydrazine extremely limit its application in large scale production.<sup>148</sup> It is hence essential to develop a relatively simple precursor route using less toxic solvents with comparable performance to those made from hydrazine based approaches.

**4.2.1. Nanoparticle based precursors.** During the past five years, there has been a rapid development in the field of nanoparticle based approach for fabrication of kesterite-based solar cells.<sup>149–153</sup> Among all the hydrazine-free approaches to fabricate CZTSSe devices, the highest efficiency kesterite solar cells were reported based on using a nanoparticulate-based solution with a maximum PCE of 10.2%;<sup>154</sup> this is rather a close value to the 12% record CZTSSe solar cell fabricated by a hydrazine-based precursor solution. Since the first reported work in 2009 employing CZTS nanoparticles, produced by a hot

injection method, to fabricate thin film kesterite solar cells,<sup>153</sup> research in this field did draw a tremendous amount of attention. The efficiency was steadily increased from PCEs < 1% to 10.2% until 2012.<sup>145,149,154</sup> In 2009, Guo *et al.*<sup>153</sup> reported a CZTSSe solar cell with an efficiency of 0.8% using pre-synthesized CZTS nanocrystals deposited on Mo substrates and a subsequent high temperature annealing in a Se atmosphere. At the same year and by optimizing the Cu/(Zn + Sn) and Zn/Sn ratios, the same group improved the solar cell efficiency to 7.2%.<sup>149</sup> The performance of solar cells was shown to be strongly dependent on the specific CZTS composition (Cu-poor and Zn-rich films usually tend to show higher device efficiency). The precise control of the final film composition, however, appeared to be difficult when quaternary CZTS nanoparticles were used as the starting precursor. Recently, Cao *et al.*<sup>151</sup> reported another fabrication route based on the use of binary ZnS and ternary  $\text{Cu}_2\text{SnS}_3$  (CTS) nanoparticles, allowing facile control of the final film composition with promising solar cell efficiencies of 8.5% (Fig. 18). Similar high device efficiencies were achieved by alloying CZTS with Ge nanoparticles;<sup>155</sup> by carefully controlling the relative cation ratios, this effective band-gap engineering resulted in CZTGeSSe solar cells with a slightly higher  $V_{\text{oc}}$  of 464 mV.

Similar to the particulate-based methods used for fabrication of CIGS devices, a mixture of metallic and metallic chalcogenide nanoparticles was used to form kesterite CZTS films. Based on a precursor solution containing a powder mixture of  $\text{Cu}_2\text{S}$ , Zn, Sn, and S nanoparticles dispersed in ethanol, Woo *et al.*<sup>156</sup> reported the fabrication of CZTS solar cells with the highest PCE of 5.14%.

Despite all these promising reports, there are still some unsolved problems concerning the use of nanoparticles. One major issue is related to the carbon residues remaining in the final film after high temperature selenization or sulfurization, promoting formation of a small-grained inter-layer in the film. Another problem is the trade-off between impurities left after the decomposition of the ligands and the need for high-quality dispersion precursors. To address the above issues, Carrete *et al.*<sup>157</sup> developed a multistrategy ligand exchange approach in the solution phase to remove the organic ligands. In this work,



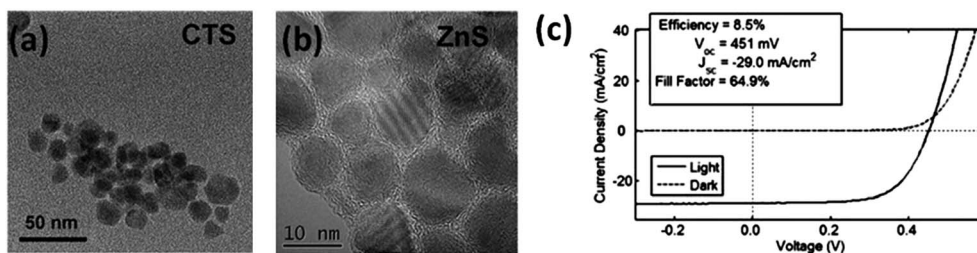


Fig. 18 TEM pictures of (a) CTS and (b) ZnS nanoparticles and the corresponding (c)  $J$ - $V$  curves of CZTSSe devices. Reprinted with permission from ref. 151, Copyright 2012 American Chemical Society.

they introduced an antimony salt to displace the organic ligands from the surface of CZTS nanoparticles (see Fig. 19, a schematic picture describing the ligand-exchange). Moreover, antimony effectively reduced the material melting point that promoted the diffusion-controlled crystallization. With an automated pulsed spray deposition followed by selenization treatment, homogeneous and carbon-free CZTSSe thin films were fabricated.

The current knowledge of particle synthesis allows the preparation of CZTS and CZTSe nanoparticles with a fine crystal structure and favorable chemical composition in various organic solvents; this makes the direct deposition of such nanoparticles at low processing temperatures feasible without high temperature selenization or sulfurization. The ultimate goal of this approach is to develop nanoparticle inks to deposit inorganic thin films under ambient or mild processing conditions, ideally in a high-throughput printing process, like a roll-to-roll process on flexible substrates. Recently, there have been some reports focusing on low temperature processing of CZTS nanoparticles. Korgel group reported a device efficiency of 0.23% utilizing the Au/CZTS/CdS/ZnO/ITO device structure without any post-thermal annealing process.<sup>152</sup> The cause of such low device efficiency is largely due to the existence of insulating organic ligands on the large surface areas of CZTS nanoparticles, inhibiting the effective charge transport between the particles. Exchanging the long chain of the capping agent oleylamine by the short ligand pyridine and employing a solar cell architecture of ITO/CZTS/PCBM/Ca/Al, Saha *et al.*<sup>158</sup> demonstrated CZTS solar cells with an improved PCE of 0.9%.

Further improvement in device efficiencies can be expected by implementing effective approaches to overcome the presence of insulating organic ligands and to passivate the various trap sites on the particle surface.

**4.2.2. Molecular based precursors.** In the non-hydrazine molecular based precursor approach, one major concern is that the transition from a mixed metallic oxide or salt precursors to a single-phase multinary sulfide/selenide material may lack sufficient reaction efficiency. However, if one can well control this transition, reasonably high-performance devices can be demonstrated. Recently, there are two groups who reported high efficiency solar cells using non-hydrazine solvents. PCEs of 6% and 7.4% were reported based on using a mixture of ethanol solution with butyldithiocarbamic acid<sup>159</sup> and DMSO,<sup>160</sup> respectively. The use of a binder-free DMSO solution was reported for the first time by Ki *et al.*,<sup>161</sup> demonstrating solar cells with a PCE of 4.1%. With some small modifications of processing, Schnabel *et al.*<sup>160</sup> significantly improved the device efficiency from 4.1% to 7.5%. The main modifications were made on post-thermal treatment and the phase-transformation process. The drying temperature was lowered from 580 °C to 300 °C and the selenization profile was modified from 500 °C, 20 min to 540 °C, 6 min. Owing to a shorter selenization time used, the problem with Sn loss was to a large extent solved and a homogeneous chemical composition was ensured. The cross-section SEM image of the CZTSSe film showed that the highly crystalline phase only forms on the top and bottom of the film, where no large grains can be found in the middle of the absorber layer, thus forming a trilayer-like structure (see

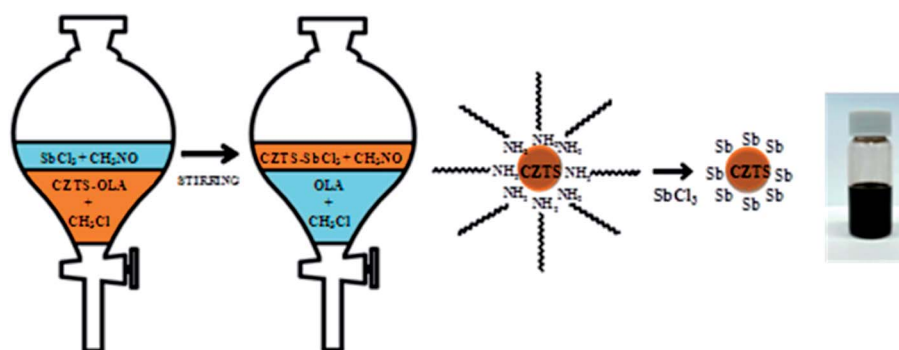


Fig. 19 Schematized view of the procedure representing the ligand-exchange of the long-chain OLA ligand with an inorganic salt  $\text{SbCl}_3$ . Reprinted with permission from ref. 157, Copyright 2013 American Chemical Society.



Fig. 20(b)). These observations point to the possibilities of improving the device performance even further by modifying the processing route and the phase transformation profile.

Wang *et al.*<sup>159</sup> employed a molecular precursor solution comprised of a mixture of binary metallic precursor oxides of  $\text{Cu}_2\text{O}$ ,  $\text{ZnO}$ , and  $\text{SnO}$  dissolved in a mixture of ethanol solution with butyldithiocarbamic acid, a similar method to the one developed for fabrication of high quality CIGS<sub>Se</sub> layers.<sup>73,74</sup> By optimizing the composition of CZTSe, solar cells with a device efficiency of 6.03% have been achieved. The advantage of this approach is the use of volatile less toxic ethanol as the main solvent and the formation of the CZTS phase at relatively low temperatures of 320 °C without any formation of binary and ternary chalcogenide phases.

**4.2.3. Hybrid particles/precursor.** Recently, Zong *et al.*<sup>162</sup> reported an interesting hydrazine-free fabrication route similar to the hydrazine-based hybrid approach proposed by Mitzi *et al.*<sup>145</sup> but using a significantly less toxic solvent propylmercaptan (PM). The ink comprises of a Zn-PM precursor based solution mixed with the pre-formed readily dispersible ternary  $\text{Cu}_2\text{SnS}_3$  (CTS) nanoparticles. Fig. 21(a) represents the schematic picture describing the formation of CTS nanoparticles, prepared by parallel dissolution of copper chloride, tin chloride and elemental S. Taking advantage of pre-formed CTS particles, the reaction pathway was effectively shortened, and the formation of undesired secondary phases was also avoided. After the film deposition, the absorber film was selenized at 450–550 °C for 60 min to complete the phase transformation to the targeted CZTSe phase. Solar cells based on this absorber layer exhibited a  $V_{\text{oc}}$  of 440 mV,  $J_{\text{sc}}$  of 32.1 mA

$\text{cm}^{-1}$  and FF of 51.9%, resulting in a solar cell with a PCE of 7.4%. Due to the simplicity and flexibility in this fabrication approach, *i.e.* the use of more environmentally benign solvent, avoiding a complex synthesis route for preparing the ternary CTS nanoparticles, and flexibility in controlling the composition and stoichiometry, this method has the potential to match the requirements for a scalable production through printing and roll-to-roll fabrication methods.

## 5. Summary and outlook

Depending on the method of preparation, Fig. 22 compares the absolute efficiency of the most efficient solution processed chalcopyrite solar cells published within the last five years, indicating a clear trend to better device efficiencies. The record published PCE of 15.2% based on the pure solution deposition,<sup>49</sup> and the certified 17.1% printed CIGSe solar cell on flexible foil announced by Nanosolar,<sup>163</sup> show the promising path of this technology, bridging the performance gap with the highest efficiency vacuum-based devices with a PCE of 20.4%.<sup>5</sup> A similar progress can be also realized in the field of solution processed kesterite solar cells with reported maximum efficiencies of 10.2% for hydrazine-free processes and 12% for the hydrazine-based approach. Although the most efficient solution processed solar cells still belong to the category of hydrazine-based devices, with plenty of studies recently concentrating on non-hydrazine based devices, there has been also a rapid progress towards efficient hydrazine-free solar cells. As shown in Fig. 22, this progress can be clearly seen for both particulate and precursor-based devices. By summarizing the results in Tables 2–5, one can see that most of the studies employ high temperature selenization or sulfurization, where only sporadic studies reported solar cells without a high temperature crystallization process. The complex post-treatments and high temperature processing routes are the important cost-driving factors for the production of solar cell technology. The high temperature routes impose not only high energy costs, but also prohibit the use of cheap substrates needed for the low-cost solar cell fabrication. With further emphasis on the low temperature processing routes, the green formulations and ongoing focus on kesterite solar cells as an excellent replacement containing only

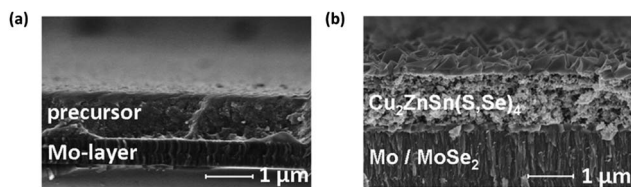


Fig. 20 Cross-sectional SEM pictures of (a) the as-deposited precursor-based film and (b) the corresponding selenized sample. Reprinted with permission from ref. 160, Copyright 2012 Elsevier B.V.

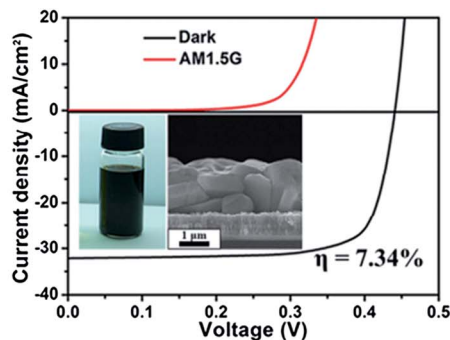
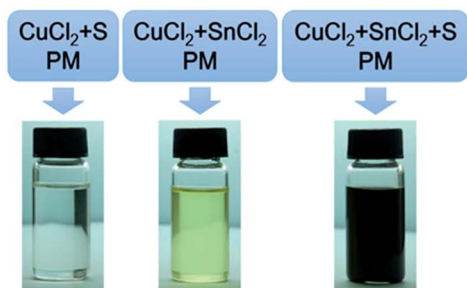


Fig. 21 (a) The preparation schematic and photographs of the parallel experiments to synthesize the CTS nanoparticles and (b) the  $I$ - $V$  characteristic of a CZTSe solar cell prepared by using a hydrazine-free hybrid particles/precursor solution (the inset shows the corresponding cross-section SEM image of the selenized CZTSe layer). Reprinted with permission from ref. 162, Copyright 2013, The Royal Society of Chemistry.





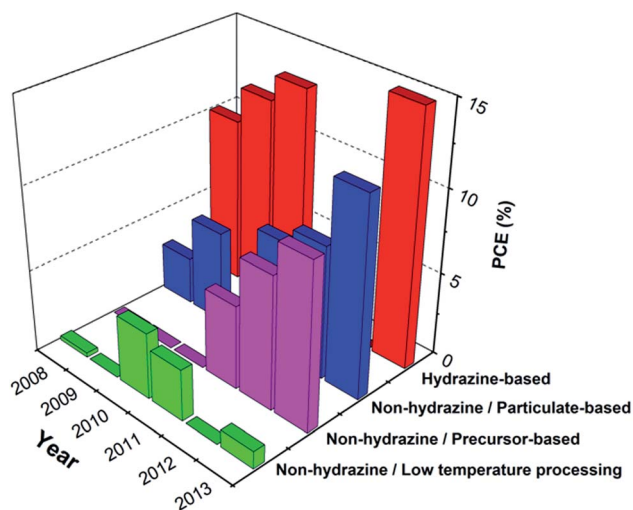


Fig. 22 Comparison of the absolute efficiency of most efficient hydrazine-based (red), non-hydrazine/particulate-based (blue), non-hydrazine/precursor-based (pink), and non-hydrazine/low temperature processed (green) solution processed chalcopyrite solar cells, published during the last five years.

earth-abundant elements, printable multicomponent inorganic inks can lead to inexpensive fabrication for light absorbing thin films. To make this possible, significant amount of investigation seems to be still necessary to unravel the complexity in the synthesis chemistry, dissolution mechanisms, drying kinetics and phase formation of thin films and their relationship to various loss mechanisms in photovoltaic devices. The pace of development can be accelerated with the emergence of new concepts and an increasing attention on hybrid structures.

## Acknowledgements

The authors would like to acknowledge the funding of the Deutsche Forschungsgemeinschaft (DFG) through the Cluster of Excellence Engineering of Advanced Materials. They also acknowledge BAYER Technology Services and Solar-Fabrik AG for financial support.

## References

- 1 National Renewable Energy Laboratory, NREL. National solar energy roadmap. In Series Management Reports. 2007, NREL/MP-520-41733/41741.

Table 5 Non-exhaustive survey of solution processed kesterite-based solar cells alongside the summary of the device parameters and information on precursor materials and preparation process

Year	Absorber	$J_{sc}$ ( $\text{mA cm}^{-2}$ )	$V_{oc}$ (mV)	FF (%)	PCE (%)	Deposition and solvent	Post-treatment	Description	Ref.
2013	CZTSSe	34.8	498	69.5	12.0	Spin-coating, hydrazine	n.a.	n.a.	147
2012	CZTSSe	34.5	460	69.8	11.1	Spin-coating, hydrazine	>500 °C (annealing with varying the concentration of S in the atm.)	A mixture of metallic chalcogen precursors and Zn NPs	145
2012	CZTSSe	32.3	409	61.0	8.1	Spin-coating, hydrazine	500 °C (under different chalcogen vapor S, S + Se and Se)	A mixture of metallic chalcogen precursors	146
2012	CZTSSe	32.8	459	68.0	10.2	n.a.	n.a.	n.a.	154
2012	CZTSSe	29	451	64.9	8.5	Spin-coating, hexanethiol	Selenization in a graphite box	Binary and ternary NPs of CTS, ZnS, and SnS	151
2012	CZTGeSSe	28.1	464	62.0	8.4	Doctor-blading, hexanethiol	500 °C (selenization in a graphite box)	CZTGeSSe particles in OLA	155
2012	CZTS	18.9	517	52.8	5.1	Spin-coating, ethanol	400–530 °C (sulfurization in $\text{N}_2 + \text{H}_2\text{S}$ (5%) atm.)	Nanosized powder of $\text{Cu}_2\text{S}$ , Zn, Sn, and S (milling process)	156
2009	CZTS	1.95	321	37.0	0.23	Spray-coating, chloroform	No annealing	$\text{Cu}(\text{acac})_2$ , zinc acetate $\text{SnCl}_2$ and S in OLA	152
2012	CZTS	5.30	390	43.0	0.90	Spin-coating, toluene	No annealing (solid state ligand exchange by pyridine)	$\text{CuCl}_2$ , $\text{ZnCl}_2$ , $\text{SnCl}_4$ and S in OLA	158
2013	CZTSSe	33.7	440	55	7.5	Doctor-blading, DMSO	540 °C (selenization in a home-made halogen-lamp-heated furnace)	$\text{Cu}(\text{OAc})_2$ , $\text{ZnCl}_2$ , $\text{SnCl}_4$ and thiourea in DMSO, binder-free	160
2013	CZTS	17.5	180	32.8	6.0	Spin-coating, ethanol with BDCA	540 °C (samples and Se powder were sealed in a hard test tube)	A mixture of metallic oxide NPs	159
2013	CZTSSe	32.6	457	66.1	7.4	Spin-coating, PM	450–550 °C (under different chalcogen vapors S, S + Se and Se)	CTS particles mixed with $\text{ZnCl}_2$	162

n.a. = not available, OLA = oleylamine.



- 2 C. Candelise, M. Winkler and R. Gross, *Prog. Photovolt: Res. Appl.*, 2012, **20**, 816–831.
- 3 C. J. Brabec, *Sol. Energy Mater. Sol. Cells*, 2004, **83**, 273.
- 4 P. Jackson, D. Hariskos, E. Lotter, S. Paetel, R. Wuerz, R. Menner, W. Wischmann and M. Powalla, *Prog. Photovolt: Res. Appl.*, 2011, **19**, 894–897.
- 5 A. Chirilă, P. Reinhard, F. Pianezzi, P. Bloesch, A. R. Uhl, C. Fella, L. Kranz, D. Keller, C. Gretener, H. Hagendorfer, D. Jaeger, R. Erni, S. Nishiwaki, S. Buecheler and A. N. Tiwari, *Nat. Mater.*, 2013, **12**, 1107–1111.
- 6 C. J. Hibberd, E. Chassaing, W. Liu, D. B. Mitzi, D. Lincot and a. N. Tiwari, *Prog. Photovoltaics Res. Appl.*, 2010, **18**, 434–452.
- 7 V. S. Saji, I.-H. Choi and C.-W. Lee, *Sol. Energy*, 2011, **85**, 2666–2678.
- 8 J.-F. Guillemoles, P. Cowache, A. Lusson, K. Fezzaa, F. Boisivon, J. Vedel and D. Lincot, *J. Appl. Phys.*, 1996, **79**, 7293.
- 9 M. A. Green, K. Emery, Y. Hishikawa, W. Warta and E. D. Dunlop, *Prog. Photovolt: Res. Appl.*, 2013, **21**, 827–837.
- 10 R. Scheer, H.-W. Schock, *Chalcogenide Photovoltaics: Physics, Technologies, and Thin Film Devices*, WILEY-VCH Verlag & Co. KGaA 2011.
- 11 J. Nelson, *The Physics of Solar Cells*, Imperial College Press, London 2003.
- 12 A. Chirilă, S. Buecheler, F. Pianezzi, P. Bloesch, C. Gretener, A. R. Uhl, C. Fella, L. Kranz, J. Perrenoud, S. Seyrling, R. Verma, S. Nishiwaki, Y. E. Romanyuk, G. Bilger and A. N. Tiwari, *Nat. Mater.*, 2011, **10**, 857–861.
- 13 U. Rau and H. W. Schock, *Appl. Phys. A*, 1999, **69**, 131.
- 14 S. Siebentritt, *Sol. Energy Mater. Sol. Cells*, 2011, **95**, 1471.
- 15 S. Siebentritt, M. Igalson, C. Persson and S. Lany, *Prog. Photovoltaics Res. Appl.*, 2010, **18**, 390.
- 16 U. Rau, K. Taretto and S. Siebentritt, *Appl. Phys. A*, 2008, **96**, 221.
- 17 M. Gloeckler, J. R. Sites and W. K. Metzger, *J. Appl. Phys.*, 2005, **98**, 113704.
- 18 K. Taretto and U. Rau, *J. Appl. Phys.*, 2008, **103**, 094523.
- 19 D. Schmid, M. Ruckh and H. W. Schock, *Sol. Energy Mater. Sol. Cells*, 1996, **41–42**, 281.
- 20 J. Li, D. B. Mitzi, V. B. Shenoy and V. B. Shenoy, *ACS Nano*, 2011, **5**, 8613.
- 21 S.-H. Wei, S. B. Zhang and A. Zunger, *Appl. Phys. Lett.*, 1998, **72**, 3199.
- 22 M. J. Romero, H. Du, G. Teeter, Y. Yan and M. M. Al-Jassim, *Phys. Rev. B: Condens. Matter Mater. Phys.*, 2011, **84**, 165324.
- 23 S. Chen, A. Walsh, X.-G. Gong and S.-H. Wei, *Adv. Mater.*, 2013, **25**, 1522.
- 24 S. Chen, X. G. Gong, A. Walsh and S.-H. Wei, *Appl. Phys. Lett.*, 2010, **96**, 021902.
- 25 C.-H. Chung, S.-H. Li, B. Lei, W. Yang, W. W. Hou, B. Bob and Y. Yang, *Chem. Mater.*, 2011, **23**, 964.
- 26 J. Alvarez-García, E. Rudigier, N. Rega, B. Barcones, R. Scheer, a. Pérez-Rodríguez, a. Romano-Rodríguez and J. R. Morante, *Thin Solid Films*, 2003, **431–432**, 122–125.
- 27 E. Rudigier, I. Luck and R. Scheer, *Appl. Phys. Lett.*, 2003, **82**, 4370.
- 28 H. Azimi, T. Heumüller, A. Gerl, G. Matt, P. Kubis, M. Distaso, R. Ahmad, T. Akdas, M. Richter, W. Peukert and C. J. Brabec, *Adv. Energy Mater.*, 2013, **3**, 1589.
- 29 I. Oja, M. Nanu, a. Katerski, M. Krunka, a. Mere, J. Raudoja and a. Goossens, *Thin Solid Films*, 2005, **480–481**, 82–86.
- 30 A.-J. Cheng, M. Manno, a. Khare, C. Leighton, S. a. Campbell and E. S. Aydil, *J. Vac. Sci. Technol.*, A, 2011, **29**, 051203.
- 31 A. Walsh, S. Chen, S.-H. Wei and X.-G. Gong, *Adv. Energy Mater.*, 2012, **2**, 400.
- 32 P. a. Fernandes, P. M. P. Salomé and a. F. da Cunha, *Thin Solid Films*, 2009, **517**, 2519.
- 33 R. Ahmad, M. Distaso, H. Azimi, C. J. Brabec and W. Peukert, *J. Nanopart. Res.*, 2013, **15**, 1886.
- 34 X. Fontané, L. Calvo-Barrio, V. Izquierdo-Roca, E. Saucedo, a. Pérez-Rodríguez, J. R. Morante, D. M. Berg, P. J. Dale and S. Siebentritt, *Appl. Phys. Lett.*, 2011, **98**, 181905.
- 35 F. Hergert, R. Hock, a. Weber, M. Purwins, J. Palm and V. Probst, *J. Phys. Chem. Solids*, 2005, **66**, 1903.
- 36 C. von Klopman, J. Djordjevic and R. Scheer, *J. Cryst. Growth*, 2006, **289**, 113.
- 37 A. Fischereder, T. Rath, W. Haas, H. Amenitsch, D. Schenk, A. Zankel, R. Saf, F. Hofer and G. Trimmel, *ACS Appl. Mater. Interfaces*, 2012, **4**, 382.
- 38 V. Izquierdo-Roca, A. Shavel, E. Saucedo, S. Jaime-Ferrer, J. Álvarez-García, A. Cabot, A. Pérez-Rodríguez, V. Bermudez and J. R. Morante, *Sol. Energy Mater. Sol. Cells*, 2011, **95**, S83.
- 39 K. Topper, J. Bruns, R. Scheer, M. Weber, a. Weidinger and D. Bräunig, *Appl. Phys. Lett.*, 1997, **71**, 482.
- 40 F. Luckert, D. I. Hamilton, M. V. Yakushev, N. S. Beattie, G. Zoppi, M. Moynihan, I. Forbes, a. V. Karotki, a. V. Mudryi, M. Grossberg, J. Krustok and R. W. Martin, *Appl. Phys. Lett.*, 2011, **99**, 062104.
- 41 J. Raudoja and M. Altosaar, *Sol. Energy Mater.*, 2003, **79**, 401.
- 42 M. Burgelman, F. Engelhardt, J. F. Guillemoles, R. Herberholz, M. Igalson, R. Klenk, M. Lampert, T. Meyer, V. Nadenau, A. Niemegeers, J. Parisi, U. Rau, H. W. Schock, M. Schmitt, O. Seifert, T. Walter and S. Zott, *Prog. Photovolt: Res. Appl.*, 1997, **5**, 121–130.
- 43 A. Jasenek, U. Rau, V. Nadenau and H. W. Schock, *J. Appl. Phys.*, 2000, **87**, 594.
- 44 R. Knecht, M. S. Hammer, J. Parisi and I. Riedel, *Phys. Status Solidi*, 2013, **210**, 1392–1399.
- 45 J. P. Leitão, N. M. Santos, P. a. Fernandes, P. M. P. Salomé, a. F. da Cunha, J. C. González, G. M. Ribeiro and F. M. Matinaga, *Phys. Rev. B: Condens. Matter Mater. Phys.*, 2011, **84**, 024120.
- 46 S. Siebentritt and S. Schuler, *J. Phys. Chem. Solids*, 2003, **64**, 1621.
- 47 O. Gunawan, T. K. Todorov and D. B. Mitzi, *Appl. Phys. Lett.*, 2010, **97**, 233506.
- 48 S. Shirakata and T. Nakada, *Thin Solid Films*, 2007, **515**, 6151–6154.
- 49 T. K. Todorov, O. Gunawan, T. Gokmen and D. B. Mitzi, *Prog. Photovolt: Res. Appl.*, 2013, **21**, 82–87.
- 50 J. B. Li, V. Chawla and B. M. Clemens, *Adv. Mater.*, 2012, **24**, 720–723.



- 51 Z. Zhang, X. Tang, U. Lemmer, W. Witte, O. Kiowski, M. Powalla and H. Hölscher, *Appl. Phys. Lett.*, 2011, **99**, 042111.
- 52 *Advanced Characterization Techniques for Thin Film Solar Cells*, ed. Daniel Abou-Ras, Thomas Kirchartz and Uwe Rau, WILEY-VCH Verlag & Co. KGaA, 2011.
- 53 K. Durose, S. E. Asher, W. Jaegermann, D. Levi, B. E. McCandless, W. Metzger, H. Moutinho, P. D. Paulson, C. L. Perkins, J. R. Sites, G. Teeter and M. Terheggen, *Prog. Photovoltaics Res. Appl.*, 2004, **12**, 177–217.
- 54 S. Ahn, C. Kim, J. H. Yun, J. Gwak, S. Jeong, B.-H. Ryu and K. Yoon, *J. Phys. Chem. C*, 2010, **114**, 8108–8113.
- 55 C. Jiang, J. Lee, D. V. Talapin and J. Am, *Chem. Soc.*, 2012, **134**, 5010–5013.
- 56 *Solution Processing of Inorganic Materials*, ed. David B. Mitzi, John Wiley & Sons, Inc, 2009.
- 57 D. B. Mitzi, *Adv. Mater.*, 2009, **21**, 3141.
- 58 T. Todorov and D. B. Mitzi, *Eur. J. Inorg. Chem.*, 2010, 17–28.
- 59 B. Bob, B. Lei, C.-H. Chung, W. Yang, W.-C. Hsu, H.-S. Duan, W. W.-J. Hou, S.-H. Li and Y. Yang, *Adv. Energy Mater.*, 2012, **2**, 504–522.
- 60 D. B. Mitzi, M. Yuan, W. Liu, A. J. Kellock, S. J. Chey, L. Gignac and A. G. Schrott, *Thin Solid Films*, 2009, **517**, 2158–2162.
- 61 D. B. Mitzi, M. Yuan, W. Liu, A. J. Kellock, S. J. Chey, V. Deline and A. G. Schrott, *Adv. Mater.*, 2008, **20**, 3657–3662.
- 62 W. Liu, D. B. Mitzi, M. Yuan, A. J. Kellock, S. J. Chey and O. Gunawan, *Chem. Mater.*, 2010, **22**, 1010.
- 63 H. Zhou, C.-J. Hsu, W.-C. Hsu, H.-S. Duan, C.-H. Chung, W. Yang and Y. Yang, *Adv. Energy Mater.*, 2012, **3**, 328–336.
- 64 M. Kaelin, D. Rudmann, F. Kurdesau, H. Zogg, T. Meyer and a. N. Tiwari, *Thin Solid Films*, 2005, **480–481**, 486–490.
- 65 A. R. Uhl, Y. E. Romanyuk and A. N. Tiwari, *Thin Solid Films*, 2011, **519**, 7259.
- 66 A. R. Uhl, C. Fella, A. Chirilă, M. R. Kaelin, L. Karvonen, A. Weidenkaff, C. N. Borca, D. Grolimund, Y. E. Romanyuk and A. N. Tiwari, *Prog. Photovolt: Res. Appl.*, 2012, **20**, 526–533.
- 67 S. J. Park, J. W. Cho, J. K. Lee, K. Shin, J. Kim and B. K. Min, *Prog. Photovolt.: Res. Appl.*, 2014, **22**, 122–128.
- 68 W. Wang, Y.-W. Su and C. Chang, *Sol. Energy Mater. Sol. Cells*, 2011, **95**, 2616–2620.
- 69 W. Wang, S.-Y. Han, S.-J. Sung, D.-H. Kim and C.-H. Chang, *Phys. Chem. Chem. Phys.*, 2012, **14**, 11154–11159.
- 70 S. Ahn, T. H. Son, A. Cho, J. Gwak, J. H. Yun, K. Shin, S. K. Ahn, S. H. Park and K. Yoon, *ChemSusChem*, 2012, **5**, 1773–1777.
- 71 B. D. Weil, S. T. Connor and Y. Cui, *J. Am. Chem. Soc.*, 2010, **132**, 6642.
- 72 L. Li, N. Coates and D. Moses, *J. Am. Chem. Soc.*, 2010, **132**, 22.
- 73 G. Wang, S. Wang, Y. Cui and D. Pan, *Chem. Mater.*, 2012, **24**, 3993–3997.
- 74 W. Zhao, Y. Cui and D. Pan, *Energy Technol.*, 2013, **1**, 131.
- 75 A. Goossens and J. Hofhuis, *Nanotechnology*, 2008, **19**, 424018.
- 76 M. Krunk, O. Kijatkina, H. Rebane, I. Oja, V. Mikli and A. Mere, *Thin Solid Films*, 2002, **404**, 71.
- 77 T. Therasajohn, M. Mathew, C. Sudhakartha, K. Vijayakumar, T. Abe and Y. Kashiwaba, *Sol. Energy Mater. Sol. Cells*, 2005, **89**, 27.
- 78 M. S. Tomar and F. J. Garcia, *Thin Solid Films*, 1982, **90**, 419–423.
- 79 P. R. Ram, R. Thangaraj, A. K. Sharma and O. P. Agnihotri, *Solar Cells*, 1985, **14**, 123.
- 80 M. Nanu, J. Schoonman and A. Goossens, *Nano Lett.*, 2005, **5**, 1716.
- 81 W. Hirpo, S. Dhingra, A. C. Sutorik and M. G. Kanatzidis, *J. Am. Chem. Soc.*, 1993, **115**, 1597.
- 82 K. K. Banger, J. a. Hollingsworth, J. D. Harris, J. Cowen, W. E. Buhro and A. F. Hepp, *Appl. Organomet. Chem.*, 2002, **16**, 617.
- 83 K. K. Banger, J. Cowen and A. F. Hepp, *Chem. Mater.*, 2001, **13**, 3827–3829.
- 84 K. K. Banger, M. H.-C. Jin, J. D. Harris, P. E. Fanwick and A. F. Hepp, *Inorg. Chem.*, 2003, **42**, 7713.
- 85 M. H. Jin, K. K. Banger, C. V. Kelly, J. H. Scofield, J. S. McNatt, J. E. Dickman and A. F. Hepp, *Proceedings of the 19th European Photovoltaic Solar Energy Conference*, 4AV.1.71, 2004.
- 86 C. Kind, C. Feldmann, A. Quintilla and E. Ahlswede, *Chem. Mater.*, 2011, **23**, 5269–5274.
- 87 Y. S. Lim, J. Jeong, J. Y. Kim, M. J. Ko, H. Kim, B. Kim, U. Jeong and D.-K. Lee, *J. Phys. Chem. C*, 2013, **117**, 11930.
- 88 D. V. Talapin, J.-S. Lee, M. V. Kovalenko and E. V. Shevchenko, *Chem. Rev.*, 2010, **110**, 389–458.
- 89 C. J. Stolle, M. G. Panthani, T. B. Harvey, V. A. Akhavan and B. A. Korgel, *ACS Appl. Mater. Interfaces*, 2012, **4**, 2757.
- 90 Q. Guo, G. M. Ford, H. W. Hillhouse and R. Agrawal, *Nano Lett.*, 2009, **9**, 3060–3065.
- 91 C. B. Murray, D. J. Norris and M. G. Bawendi, *J. Am. Chem. Soc.*, 1993, **115**, 8706–8715.
- 92 G. Konstantatos, I. Howard, A. Fischer, S. Hoogland, J. Clifford, E. Klem, L. Levina and E. H. Sargent, *Nature*, 2006, **442**, 180.
- 93 J. D. Olson, G. P. Gray and S. a. Carter, *Sol. Energy Mater. Sol. Cells*, 2009, **93**, 519.
- 94 J.-J. Wang, Y.-Q. Wang, F.-F. Cao, Y.-G. Guo and L.-J. Wan, *J. Am. Chem. Soc.*, 2010, **132**, 12218.
- 95 B. L. Cushing, V. L. Kolesnichenko and C. J. O'Connor, *Chem. Rev.*, 2004, **104**, 3893.
- 96 C. Burda, X. Chen, R. Narayanan and M. A. El-Sayed, *Chem. Rev.*, 2005, **105**, 1025–1102.
- 97 H. Goesmann and C. Feldmann, *Angew. Chem., Int. Ed. Engl.*, 2010, **49**, 1362–1395.
- 98 J. Tang, S. Hinds, S. O. Kelley and E. H. Sargent, *Chem. Mater.*, 2008, **20**, 6906–6910.
- 99 M. Kruszynska, H. Bo rchert, J. Parisi and J. Kolny-Olesiak, *J. Am. Chem. Soc.*, 2010, **132**, 15976.
- 100 M. Chiang, S. Chang, C. Chen, F. Yuan and H. Tuan, *J. Phys. Chem. C*, 2011, **115**, 1592–1599.
- 101 Q. Guo, S. J. Kim, M. Kar, W. N. Shafarman, R. W. Birkmire, E. a. Stach, R. Agrawal and H. W. Hillhouse, *Nano Lett.*, 2008, **8**, 2982.



- 102 Q. Guo, G. M. Ford, R. Agrawal and H. W. Hillhouse, *Prog. Photovolt: Res. Appl.*, 2013, **21**, 64–71.
- 103 M. G. Panthani, V. Akhavan, B. Goodfellow, J. P. Schmidtke, L. Dunn, A. Dodabalapur, P. F. Barbara and B. A. Korgel, *J. Am. Chem. Soc.*, 2008, **130**, 16770–16777.
- 104 V. A. Akhavan, M. G. Panthani, B. W. Goodfellow, D. K. Reid and B. a. Korgel, *Energy Express*, 2010, **18**, A411–A420.
- 105 V. A. Akhavan, B. W. Goodfellow, M. G. Panthani, C. Steinhagen, T. B. Harvey, C. J. Stolle and B. A. Korgel, *J. Solid State Chem.*, 2012, **189**, 2–12.
- 106 M. Bär, S. Nishiwaki, L. Weinhardt, S. Pookpanratana, W. N. Shafarman and C. Heske, *Appl. Phys. Lett.*, 2008, **93**, 042110.
- 107 A. Romeo, M. Terheggen, D. Abou-Ras, D. L. Bätznner, F.-J. Haug, M. Kälin, D. Rudmann and A. N. Tiwari, *Prog. Photovolt: Res. Appl.*, 2004, **12**, 93–111.
- 108 T. Arita, N. Suyama, Y. Kita, S. Kitamura, T. Hibino, H. Takada, K. Omura, N. Ueno and M. Murozono, *Conference Record of the 20th IEEE Photovoltaic Specialists Conference*, IEEE, New York, 1988, p. 1650.
- 109 B. M. Basol, V. K. Kapur, G. Norsworthy, A. Halani, C. R. Leidholm and R. Roe, *Electrochem. Solid State Lett.*, 1998, **1**, 252.
- 110 C. Eberspacher, C. Fredric, K. Pauls and J. Serra, *Thin Solid Films*, 2001, **387**, 18–22.
- 111 G. Norsworthy, C. R. Leidholm, A. Halani, V. K. Kapur, R. Roe, B. M. Basol and R. Matson, *Sol. Energy Mater. Sol. Cells*, 2000, **60**, 127–134.
- 112 F. Roux, S. Amtablian, M. Anton, G. Besnard, L. Bilhaut, P. Bommersbach, J. Braillon, C. Cayron, a. Disdier, H. Fournier, J. Garnier, a. Jannaud, J. Jouhannaud, a. Kaminski, N. Karst, S. Noël, S. Perraud, O. Poncelet, O. Raccurt, D. Rapisarda, a. Ricaud, D. Rouchon, M. Roumanie, E. Rouviere, O. Sicardy, F. Sonier, K. Tarasov, F. Tardif, M. Tomassini and J. Villanova, *Sol. Energy Mater. Sol. Cells*, 2013, **115**, 86–92.
- 113 V. K. Kapur, A. Bansal, P. Le and O. I. Asensio, *Thin Solid Films*, 2003, **431–432**, 53.
- 114 G. Chen, L. Wang, X. Sheng, H. Liu, X. Pi and D. Yang, *J. Alloys Compd.*, 2010, **507**, 317.
- 115 J. Chang, J. H. Lee, J.-H. Cha, D.-Y. Jung, G. Choi and G. Kim, *Thin Solid Films*, 2011, **519**, 2176.
- 116 S.-H. Liu, F.-S. Chen and C.-H. Lu, *J. Alloys Compd.*, 2012, **517**, 14.
- 117 S. A. Möckel, A. Hölzing, R. Hock and P. J. Wellmann, *Thin Solid Films*, 2013, **535**, 133–137.
- 118 M. Periasamy and M. Thirumalaikumar, *J. Organomet. Chem.*, 2000, **609**, 137.
- 119 S. Jeong, B.-S. Lee, S. Ahn, K. Yoon, Y.-H. Seo, Y. Choi and B.-H. Ryu, *Energy Environ. Sci.*, 2012, **5**, 7539.
- 120 H. Min Lim, S. K. Batabyal, S. S. Pramana, L. H. Wong, S. Magdassi and S. G. Mhaisalkar, *Chem. Commun.*, 2013, **49**, 5351.
- 121 S. Ahn, K. Kim, A. Cho, J. Gwak, J. H. Yun, K. Shin, S. Ahn and K. Yoon, *ACS Appl. Mater. Interfaces*, 2012, **4**, 1530–1536.
- 122 K. Kim, Y.-J. Eo, A. Cho, J. Gwak, J. H. Yun, K. Shin, S. K. Ahn, S. H. Park, K. Yoon and S. Ahn, *J. Mater. Chem.*, 2012, **22**, 8444.
- 123 S. Ahn, Y. J. Choi, K. Kim, Y.-J. Eo, A. Cho, J. Gwak, J. H. Yun, K. Shin, S. K. Ahn and K. Yoon, *ChemSusChem*, 2013, **6**, 1282–1287.
- 124 A. Cho, S. Ahn, J. H. Yun, J. Gwak, H. Song and K. Yoon, *J. Mater. Chem.*, 2012, **22**, 17893.
- 125 Y. Cai, J. C. W. Ho, S. K. Batabyal, W. Liu, Y. Sun, S. G. Mhaisalkar and L. H. Wong, *ACS Appl. Mater. Interfaces*, 2013, **5**, 1533–1537.
- 126 J.-J. Wang, J.-S. Hu, Y.-G. Guo and L.-J. Wan, *NPG Asia Mater.*, 2012, **4**, e2.
- 127 J.-J. Wang, Y.-Q. Wang, F.-F. Cao, Y.-G. Guo and L.-J. Wan, *J. Am. Chem. Soc.*, 2010, **132**, 12218–12221.
- 128 D. J. Milliron, I. Gur and A. P. Alivisatos, *MRS Bull.*, January 2005, **30**.
- 129 H. Borchert, *Energy Environ. Sci.*, 2010, **3**, 1682.
- 130 W. Yue, S. Han, R. Peng, W. Shen, H. Geng, F. Wu, S. Tao and M. Wang, *J. Mater. Chem.*, 2010, **20**, 7570.
- 131 E. Maier, T. Rath, W. Haas, O. Werzer, R. Saf, F. Hofer, D. Meissner, O. Volobujeva, S. Bereznev, E. Mellikov, H. Amenitsch, R. Resel and G. Trimmel, *Sol. Energy Mater. Sol. Cells*, 2011, **95**, 1354.
- 132 E. Arici, N. S. Sariciftci and D. Meissner, *Adv. Funct. Mater.*, 2003, **13**, 165.
- 133 F. M. Courtel, R. W. Paynter, B. Marsan and M. Morin, *Chem. Mater.*, 2009, **21**, 3752.
- 134 M. Kruszynska, M. Knipper, J. Kolny-Olesiak, H. Borchert and J. Parisi, *Thin Solid Films*, 2011, **519**, 7374–7377.
- 135 Y. Yang, H. Zhong, Z. Bai, B. Zou, Y. Li and G. D. Scholes, *J. Phys. Chem. C*, 2012, **116**, 7280–7286.
- 136 E. Arici, H. Hoppe, F. Schäffler, D. Meissner, M. A. Malik and N. S. Sariciftci, *Thin Solid Films*, 2004, **451–452**, 612–618.
- 137 B. P. A. Van Hal, M. M. Wienk, J. M. Kroon, W. J. H. Van Gennip, P. Jonkheijm and R. A. J. Janssen, *Adv. Mater.*, 2003, **15**, 118.
- 138 S. D. Oosterhout, M. M. Wienk, S. S. van Bavel, R. Thiedmann, L. J. A. Koster, J. Gilot, J. Loos, V. Schmidt and R. a. J. Janssen, *Nat. Mater.*, 2009, **8**, 818.
- 139 T. Rath, M. Edler, W. Haas, A. Fischereder, S. Moscher, A. Schenk, R. Trattig, M. Sezen, G. Mauthner, A. Pein, D. Meischler, K. Bartl, R. Saf, N. Bansal, S. a. Haque, F. Hofer, E. J. W. List and G. Trimmel, *Adv. Energy Mater.*, 2011, **1**, 1046.
- 140 D. B. Mitzi, O. Gunawan, T. K. Todorov, K. Wang and S. Guha, *Sol. Energy Mater. Sol. Cells*, 2011, **95**, 1421.
- 141 S. Siebentritt and S. Schorr, *Prog. Photovolt: Res. Appl.*, 2012, **20**, 512–519.
- 142 D. B. Mitzi, O. Gunawan, T. K. Todorov and D. A. R. Barkhouse, *Philos. Trans. R. Soc., A*, 2013, **371**, 20110432.
- 143 A. Fairbrother, E. García-Hemme, V. Izquierdo-Roca, X. Fontané, F. a. Pulgarín-Agudelo, O. Vigil-Galán, A. Pérez-Rodríguez and E. Saucedo, *J. Am. Chem. Soc.*, 2012, **134**, 8018.





- 144 A. Redinger, D. M. Berg, P. J. Dale and S. Siebentritt, *J. Am. Chem. Soc.*, 2011, **133**, 3320.
- 145 T. K. Todorov, J. Tang, S. Bag, O. Gunawan, T. Gokmen, Y. Zhu and D. B. Mitzi, *Adv. Energy Mater.*, 2013, **3**, 34–38.
- 146 W. Yang, H.-S. Duan, B. Bob, H. Zhou, B. Lei, C.-H. Chung, S.-H. Li, W. W. Hou and Y. Yang, *Adv. Mater.*, 2012, **24**, 6323.
- 147 M. T. Winkler, W. Wang, O. Gunawan, H. J. Hovel, T. Todorov and D. B. Mitzi, *Energy Environ. Sci.*, 2014, **7**, 1029–1036.
- 148 Y. E. Romanyuk, C. M. Fella, A. R. Uhl, m. Werner, a. N. Tiwari, T. Schnabel and E. Ahlswede, *Sol. Energy Mater. Sol. Cells*, 2013, **119**, 181–189.
- 149 Q. Guo, G. M. Ford, W. C. Yang, B. C. Walker, E. A. Stach, H. W. Hillhouse and R. Agrawal, *J. Am. Chem. Soc.*, 2010, **132**, 17384.
- 150 G. M. Ford, Q. Guo, R. Agrawal and H. W. Hillhouse, *Chem. Mater.*, 2011, **23**, 2626.
- 151 Y. Cao, M. S. Denny, J. V. Caspar, W. E. Farneth, Q. Guo, A. S. Ionkin, L. K. Johnson, M. Lu, I. Malajovich, D. Radu, H. D. Rosenfeld, K. R. Choudhury and W. Wu, *J. Am. Chem. Soc.*, 2012, **134**, 15644.
- 152 C. Steinhagen, M. G. Panthani, V. Akhavan, B. Goodfellow, B. Koo and B. A. Korgel, *J. Am. Chem. Soc.*, 2009, **131**, 12554.
- 153 Q. Guo, H. W. Hillhouse and R. Agrawal, *J. Am. Chem. Soc.*, 2009, **131**, 11672.
- 154 C. Leidholm, C. Hotz, A. Breeze, C. Sunderland, and W. Ki, NREL Subcontract Report 2012, NREL/SR-5200–56510.
- 155 Q. Guo, G. M. Ford, W.-C. Yang, C. J. Hages, H. W. Hillhouse and R. Agrawal, *Sol. Energy Mater. Sol. Cells*, 2012, **105**, 132.
- 156 K. Woo, Y. Kim and J. Moon, *Energy Environ. Sci.*, 2012, **5**, 5340.
- 157 A. Carrete, A. Shavel, X. Fontané, J. Montserrat, J. Fan, M. Ibáñez, E. Saucedo, A. Pérez-Rodríguez and A. Cabot, *J. Am. Chem. Soc.*, 2013, **135**, 15982–15985.
- 158 S. K. Saha, A. Guchhait and A. J. Pal, *Phys. Chem. Chem. Phys.*, 2012, **14**, 8090.
- 159 G. Wang, W. Zhao, Y. Cui, Q. Tian, S. Gao, L. Huang and D. Pan, *ACS Appl. Mater. Interfaces*, 2013, **5**, 10042–10047.
- 160 T. Schnabel, M. Löw and E. Ahlswede, *Sol. Energy Mater. Sol. Cells*, 2013, **117**, 324.
- 161 W. Ki and H. W. Hillhouse, *Adv. Energy Mater.*, 2011, **1**, 732.
- 162 K. Zong, Y. Sun, Y. Zhang, H. Wang, J. Liu and H. Yan, *J. Mater. Chem. A*, 2013, DOI: 10.1039/c3ta13157b.
- 163 Press release: [http://www.nanosolar.com/detail\\_press/nanosolar-achieves-17-1-aperture-efficiency-through-printed-cigs-process/](http://www.nanosolar.com/detail_press/nanosolar-achieves-17-1-aperture-efficiency-through-printed-cigs-process/).

